MNRAS 000, 1–21 (2019) Preprint 28 March 2019 Compiled using MNRAS LATEX style file v3.0

Probing the extragalactic fast transient sky at minute timescales with DECam

I. Andreoni[1,2,3,4,*], J. Cooke[1,3,5], S. Webb[1,3], A. Rest[6,7], T. Pritchard[1,8], M. Caleb[1,9,10], S.-W. Chang[3,5,9], W. Farah[1], A. Lien[11,12], A. Möller[5,9], M. E. Ravasio[13,14,1] , T. M. C. Abbott[15], S. Bhandari[1,16], A. Cucchiara[17], C. Flynn[1], F. Jankowski[1,5,10], E. F. Keane[18], T. J. Moriya[19], C. A. Onken[5,9], A. Parthasarathy[1,3,16], D. C. Price[1,20], E. Petroff[21,22], S. Ryder[2,23], C. Wolf[5,9]

[1]*Swinburne University of Technology, PO Box 218, Hawthorn, VIC 3122, Australia*
[2]*Australian Astronomical Observatory, 105 Delhi Rd, North Ryde, NSW 2113, Australia*
[3]*ARC Centre of Excellence for Gravitational Wave Discovery (OzGrav), Australia*
[4]*Division of Physics, Math and Astronomy, California Institute of Technology, Pasadena, CA 91125, USA*
[5]*ARC Centre of Excellence for All-sky Astrophysics (CAASTRO)*
[6]*Space Telescope Science Institute, 3700 San Martin Dr., Baltimore, MD 21218, USA*
[7]*Department of Physics and Astronomy, Johns Hopkins University, 3400 North Charles Street, Baltimore, MD 21218, USA*
[8]*Center for Cosmology and Particle Physics, New York University, 726 Broadway, New York, NY 10004, USA*
[9]*Research School of Astronomy and Astrophysics, Australian National University, Canberra, ACT 2611, Australia*
[10]*Jodrell Bank Centre for Astrophysics, School of Physics and Astronomy, The University of Manchester, Manchester M13 9PL, UK*
[11]*Center for Research and Exploration in Space Science and Technology (CRESST) and NASA Goddard Space Flight Center, Greenbelt, MD 20771, USA*
[12]*Department of Physics, University of Maryland, Baltimore County, 1000 Hilltop Circle, Baltimore, MD 21250, USA*
[13]*Università degli Studi di Milano-Bicocca, Dipartimento di Fisica U2, Piazza della Scienza 3, Milano 20126, Italy*
[14]*INAF - Osservatorio Astronomico di Brera, via Bianchi 46, Merate 23807, Italy*
[15]*Cerro Tololo Inter-American Observatory, National Optical Astronomy Observatory, Casilla 603, 1700000 La Serena, Chile*
[16]*CSIRO Astronomy and Space Science, Australia Telescope National Facility, PO Box 76, Epping NSW 1710, Australia*
[17]*College of Science and Mathematics, University of the Virgin Islands, #2 Brewers Bay Road, Charlotte Amalie, USVI 00802*
[18]*SKA Organisation, Jodrell Bank Observatory, Macclesfield SK11 9DL, UK*
[19]*Division of Theoretical Astronomy, National Astronomical Observatory of Japan, National Institutes of Natural Sciences, 2-21-1 Osawa, Mitaka, Tokyo 181-8588, Japan*
[20]*Department of Astronomy, University of California Berkeley, Berkeley CA 94720*
[21]*Anton Pannekoek Institute for Astronomy, University of Amsterdam, Amsterdam, the Netherlands*
[22]*ASTRON, Netherlands Institute for Radio Astronomy, Dwingeloo, the Netherlands*
[23]*Department of Physics & Astronomy, Macquarie University, NSW 2109, Australia,*
[*]*E-mail: andreoni@caltech.edu*

Submitted for publication in MNRAS

ABSTRACT
Searches for optical transients are usually performed with a cadence of days to weeks, optimised for supernova discovery. The optical fast transient sky is still largely unexplored, with only a few surveys to date having placed meaningful constraints on the detection of extragalactic transients evolving at sub-hour timescales. Here, we present the results of deep searches for dim, minute-timescale extragalactic fast transients using the Dark Energy Camera, a core facility of our all-wavelength and all-messenger Deeper, Wider, Faster programme. We used continuous 20 s exposures to systematically probe timescales down to 1.17 minutes at magnitude limits $g > 23$ (AB), detecting hundreds of transient and variable sources. Nine candidates passed our strict criteria on duration and non-stellarity, 5 of which could later be classified as flare stars, but 4 of which have more unsure classification. Searches for fast radio burst and gamma-ray counterparts during simultaneous multi-facility observations yielded no counterparts to those 4 optical transients. Also, no long-term variability was detected with pre-imaging and follow-up observations using the SkyMapper optical telescope. We place (conservative) upper limits and (optimistic) measurements of minute-timescale fast optical transient rates for a range of depths and timescales. Finally, we demonstrate that optical g-band light curve behaviour alone cannot discriminate between confirmed extragalactic fast transients such as prompt GRB flashes and Galactic stellar flares.

Key words: supernovae: general – stars: flare – gamma-ray burst: general – radio continuum: transients

1 INTRODUCTION

The optical transient sky is largely unexplored at short timescales. Most successful time-domain surveys aim at detecting supernovae and variable events evolving on week or month timescales. Those include, for example, the Supernova Legacy Survey (Astier et al. 2006), the Calán/Tololo Survey (Hamuy & Pinto 1999), the Palomar Transient Factory (PTF, Rau et al. 2009), the Catalina Sky Survey (Drake et al. 2009), Pan-STARRS (Stubbs et al. 2010), the Dark Energy Survey (DES, Dark Energy Survey Collaboration et al. 2016), the All-Sky Automated Survey for Supernovae (ASAS-SN, Shappee et al. 2014; Holoien et al. 2017), and now the Asteroid Terrestrial-impact Last Alert System (ATLAS[1]) and the Zwicky Transient Facility (ZTF[2], Bellm et al. 2019) among others.

Recent work unveiled new classes of luminous, rapidly-evolving supernovae (Poznanski et al. 2010; Kasliwal et al. 2010; Drout et al. 2014; Shivvers et al. 2016; Arcavi et al. 2016; Rodney et al. 2018; Pursiainen et al. 2018; De et al. 2018) performing observations with nightly and sub-nightly cadence. Rest et al. (2018) present the most extreme of these luminous fast transients discovered to date, which shows a rise time of 2.2 days, a time above half-maximum of only 6.8 days, and a peak luminosity comparable to Type Ia supernovae. Bright optical flashes have also been observed during rapid follow up of long gamma-ray bursts using robotic telescopes (Fox et al. 2003; Cucchiara et al. 2011; Vestrand et al. 2014; Martin-Carrillo et al. 2014; Troja et al. 2017).

Rapid optical and infrared transients of high interest are kilonovae, which are associated with gravitational-wave events (e.g., Abbott et al. 2017) in addition to short gamma-ray bursts (Perley et al. 2009; Tanvir et al. 2013; Berger et al. 2013a; Gao et al. 2015; Jin et al. 2015, 2016; Troja et al. 2018; Jin et al. 2019). The discovery of a kilonova counterpart to the neutron-star merger GW170817 allowed the precise pin-pointing of the event in the sky (Coulter et al. 2017; Soares-Santos et al. 2017; Valenti et al. 2017; Arcavi et al. 2017; Lipunov et al. 2017; Tanvir et al. 2017) and allowed more than 70 facilities to monitor its evolution at many wavelengths (e.g., Abbott et al. 2017). Now we know that multiple components characterise the emission arising from mergers such as GW170817 (see for example Cowperthwaite et al. 2017; Kasliwal et al. 2017; Villar et al. 2017). In particular, observations of this transient revealed an early, blue component that evolves in about three days (with a rising phase of hours), but its origin is still unclear. Early detection and monitoring of a population of kilonovae can allow us to understand the nature of this rapidly evolving component (Arcavi 2018). As multi-messenger astronomy grows in importance, more and more surveys are dedicated to the search for kilonova-like transients (e.g., Doctor et al. 2017) or to probe the background of contaminant sources during the follow up of gravitational-wave triggers (Cowperthwaite et al. 2018).

In addition to dedicated observing campaigns, new searches for fast optical transients are performed in archival data of surveys such as DES (Pursiainen et al. 2018) and PTF (Ho et al. 2018). In the latter, the authors discovered an already-identified gamma-ray burst afterglow that was identified independently from gamma-ray triggers (Cenko et al. 2015). The Sky2Night project (van Roestel et al. 2019) searched for fast transients using PTF, with observations performed with 2 hr cadence for 8 nights. van Roestel et al. (2019) place upper limits on rates of 4 hr and 1 day timescale transients at $R < 19.7$ limiting magnitude, obtaining $R < 37 \times 10^{-4}\mathrm{deg}^{-2}\mathrm{d}^{-1}$ and $R < 9.3 \times 10^{-4}\mathrm{deg}^{-2}\mathrm{d}^{-1}$, respectively.

Only a few wide-field surveys have been carried out at timescales shorter than 1 hr. The continuous 30-minute cadence of the *Kepler* K2 project led to the first discovery of the optical shock breakout of a core-collapse supernova (Garnavich et al. 2016, but see also Rubin & Gal-Yam (2017)). If considered independently from the long-lasting supernova emission, this constitutes a rare example of hour-timescale extragalactic fast transient detection. Bersten et al. (2018) present the remarkable discovery of another optical supernova shock breakout, revealing an increase by $\Delta M_V \sim 0.6$ in ~ 25 minutes and estimated to last ~ 0.1 day. Other fast-cadenced surveys include a monitoring of the Fornax galaxy cluster (Rau et al. 2008), and blind surveys such as ROTSE III (Rykoff et al. 2005), the Deep Lens Survey (DLS, Becker et al. 2004), MASTER (Lipunov et al. 2007), and Pi of the Sky (Sokołowski et al. 2010). Results from the Pan-STARRS Medium-Deep Survey were reported by Berger et al. (2013b). The authors provided a summary of the upper limits on extragalactic fast optical transients evolving on ~0.5 hours timescales until 2013: the upper limits placed by all those surveys (Fig. 6) confirm that Galactic M-dwarf flares outnumber extragalactic fast transients by a large factor (up to several orders of magnitude, Rau et al. 2008). More recent surveys explore similar short-timescale regimes, for example the High Cadence Transient Survey (Förster et al. 2016, HiTS). Interesting detections of fast-rising transients, increasing their luminosity by > 1 magnitude in the restframe near-ultraviolet wavelengths between two consecutive nights (Tanaka et al. 2016), fuels the field of fast transient searches with exciting prospects.

Current surveys such as ZTF and Catalina Sky Survey can provide data suitable to search for minute to hour timescale transients. In the near future, the Large Synoptic Survey Telescope (LSST, LSST Science Collaboration et al. 2009) is expected to come online. LSST will survey the sky at deep magnitude limits and thanks to its large field of view ($\sim 10\,\mathrm{deg}^2$) it is expected to discover several thousands of extragalactic transients every night. The choice of the observing cadence will determine the degree to which LSST can contribute to different research areas in time domain astronomy.

This work aims to explore a new region of the optical luminosity-timescale phase space (e.g., Cenko 2017), focusing on the search for faint extragalactic transients fully evolving in minutes. We performed deep and fast-cadenced observations with the Dark Energy Camera (DECam, Flaugher et al. 2015), a wide-field imager mounted at the prime focus of the 4-m Blanco telescope at the Cerro Tololo Inter-American Observatory (CTIO) in Chile. Such observations were performed in the framework of the Deeper

[1] http://atlas.fallingstar.com/
[2] https://www.ztf.caltech.edu/

Wider Faster programme[3] (Cooke et al., in prep; Andreoni & Cooke 2018), described in the next section. Fast cadenced observations with DECam are a key optical component of DWF that enables new studies, including the search for counterparts to fast radio bursts (FRBs, Lorimer et al. 2007) at many other wavelengths. FRBs are transients detected at radio wavelengths as dispersed signals that last only a few milliseconds. Several arguments support an extragalactic origin for FRBs, including the identification of the host galaxy of the repeating burst FRB 121102 (Tendulkar et al. 2017). However, the nature of FRBs is still unknown, thus the detection of possible optical or high-energy counterparts could shed light on the FRB physics.

A subset of the total quantity of optical data collected during DWF campaigns is analysed and presented in this paper (Table 1-2). The chosen observations allow the most systematic analysis of minute-timescale fast transients over multiple nights, as the observing conditions were the most uniform of the full dataset.

The paper is organised as follows. Observations are presented in Section 2. Our analysis is described in Section 3 and its results are presented in Section 4. Searches for longer duration optical transients, FRBs, and GRBs are presented in Section 5. Rates for fast optical transients in the survey-depth transient-timescale phase space are presented in Section 6. We discuss the results in Section 7 and we conclude with a summary of this work in Section 8.

2 OBSERVATIONS

We describe the Deeper Wider Faster programme in Sec. 2.1, the criteria driving the choice of the target fields in Sec. 2.2, and the characteristics of the unique, fast-cadenced optical images in Sec. 2.3.

2.1 The Deeper Wider Faster programme

The DWF programme is designed to unveil the fastest and most elusive bursts in the sky. Identifying counterparts to FRBs constitute the primary goal of the programme. The novelty of the approach adopted by the DWF team resides in coordinating deep, wide-field, fast-cadenced observations *simultaneously* with multiple small to large all-messenger facilities. By contrast, most of the existing efforts to accomplish the same science goals rely on different observing strategies. Usually when an interesting transient is detected by the survey telescope (or neutrino and gravitational-wave detectors), then a network of facilities receives the trigger and reacts to follow up the transient. Such a *reactive* approach has several limitations, for example the multi-wavelength information is usually collected hours or days after the first detection. This causes the loss of possibly significant information or, in the case of FRBs, may be the cause of the lack of any counterpart discovered to date[4]. During DWF campaigns the fields are observed at multiple wavelengths in a *proactive* way: before, during, and after minute- and sub-minute-timescale fast transients shine. Rapid detection and prompt and long-term follow up of transients is key to the success of the programme. Blanco/DECam has been the core optical facility during the first five DWF observing runs (2 pilot and 3 operational runs), spanning between January 2015 and February 2017.

By 2018, the DWF programme has grown and now has more than 40 participating facilities, including the Subaru/Hyper Suprime-Cam (HSC) used as the core optical instrument for simultaneous observations in February 2018. The thorough analysis of the Subaru and the multi-wavelength data will be presented in future publications.

2.2 Target fields

Coordinating multiple telescopes that shadow each other constrains the region of sky observable during simultaneous observations. Such limitations become particularly significant when the observatories are located on different continents. In fact, the ground-based core facilities used during DWF from 2015 to 2017 for simultaneous or rapid follow-up observations are located in Chile (Blanco/DECam, Rapid Eye Mount telescope, Gemini-South) and in Australia (Parkes, Molonglo, ATCA, and SkyMapper). Constraints change when using core facilities other than DECam and Australian radio telescopes for DWF observations, for example when using Subaru/HSC in Hawaii, or the MeerKAT radio telescope in South Africa in the near future. For space-based observatories such as *Swift*, constraints include limited time on fields far from the poles, earth occultation times, and Sun constraints.

We demonstrated that these specific geographical constraints can be overcome (Cooke et al., in prep) and successful DWF observations from Chile and Australia can be performed all year around. We chose the target fields in relation to the following criteria:

- Sky locations where FRBs were previously discovered (here FRB131104). The field of view of the 13-beam receiver at Parkes (see Section 5.2) well matches the DECam field of view (FoV) but, in addition, the localisation error for those FRBs discovered with Parkes (~15′ diameter) allows targeted, simultaneous observations using telescopes with FoV smaller than DECam, such as REM and *Swift*/UVOT-XRT;
- Nearby galaxy clusters (e.g., Antlia), nearby galaxies, or globular clusters;
- Legacy fields (e.g., COSMOS field) having dense photometric and spectroscopic information in multiple wavelengths and space-based high resolution imaging; and/or fields where we have previous DECam deep imaging and colour information, located at high Galactic latitude and observable for $\gtrsim$1 hr from Chile and Australia (Prime, 3hr, 4hr).

More than 15 fields were observed with high-cadence

[3] http://dwfprogram.altervista.org/

[4] Hardy et al. (2017) report upper limits on optical flux at times coincident with bursts from the repeating FRB 121102. The extremely fast cadence of Thai National Telescope/ULTRASPEC (70.7 ms frames) makes their results meaningful, however we caution that *i)* possible optical emission could have been fainter than the 5σ upper limit of ULTRASPEC ($m_i \sim 15.75$, AB), and *ii)* FRB 121102 may not be representative of the whole FRB population.

Table 1. Equatorial (J2000) and Galactic coordinates of the target fields selected for this work, from a larger DWF dataset.

Target Field	RA	Dec	l	b
3hr	03:00:00	−55:25:00	272.47784°	−53.43243°
4hr	04:10:00	−55:00:00	264.94437°	−44.75641°
Prime	05:55:07	−61:21:00	270.35527°	−30.26267°
FRB131104	06:44:00	−51:16:00	260.53726°	−21.94809°
Antlia	10:30:00	−35:20:00	272.94307°	−19.17249°

simultaneous observations during DWF observing runs. Table 1 reports the coordinates of target fields whose data are analysed in this work.

2.3 Fast-cadence imaging with DECam

DWF observing campaigns have produced a large quantity of multi-wavelength data. These are analysed in real time or near-real time to search for FRBs, their possible counterparts, and to discover Galactic and extragalactic fast transients. DWF collected $\gtrsim 10,000$ optical images with DECam, mainly in the g filter, which allows ~ 0.5 mag deeper observations in comparison with other filters. The expected depth for 20 s exposure in g-band is 23.7 magnitudes (AB), against 22.6, 23.1, 22.6, and 21.6 magnitudes of the u-r-i-z filters, respectively (1.0 arcsec FWHM seeing). Typical seeing and relatively high airmass (~1.5) required for the coordinated observations can affect these values, sometimes moving the g-band limiting magnitude closer to ~23 mag.

The observing strategy with DECam during DWF runs is based on a series of continuous exposures. Telescope movements are limited to a few arcseconds in order to cover the largest common area of the sky with adjacent exposures. In this work we analyse 25.76 hr of high-cadenced images: 20 s continuous exposures in g band, separated by ~30 s where CCDs complete the readout and the new exposures start. Each image covers an effective field of view of 2.52 deg^2, accounting for CCD gaps and the frame area cropped during the alignment of the images. Details of the observations discussed in this work are presented in Table 2. Data are processed and calibrated with the NOAO High-Performance Pipeline System (Valdes & Swaters 2007; Swaters & Valdes 2007).

The high cadence of our images allows us to study transient and variable events in great detail. For example, the structure of the stellar flare DWF17l in Figure 1, sampled at 50 s intervals (20 s exposure + 30 s overhead), is lost when median-stacking sets of 9 consecutive images, equating to ~ 7 min intervals. Similarly, fast-cadence imaging reveals a non-monotonic fade of the light curve of DWF17ax, difficult to study at slower cadence (Figure 2).

3 ANALYSIS: SEARCH FOR EXTRAGALACTIC FAST TRANSIENT CANDIDATES

Data are searched using the custom *Mary* pipeline (Andreoni et al. 2017). The pipeline aids discovery of optical transients with image subtraction techniques, processing all CCDs in parallel with the Green II (g2) supercomputer at Swinburne

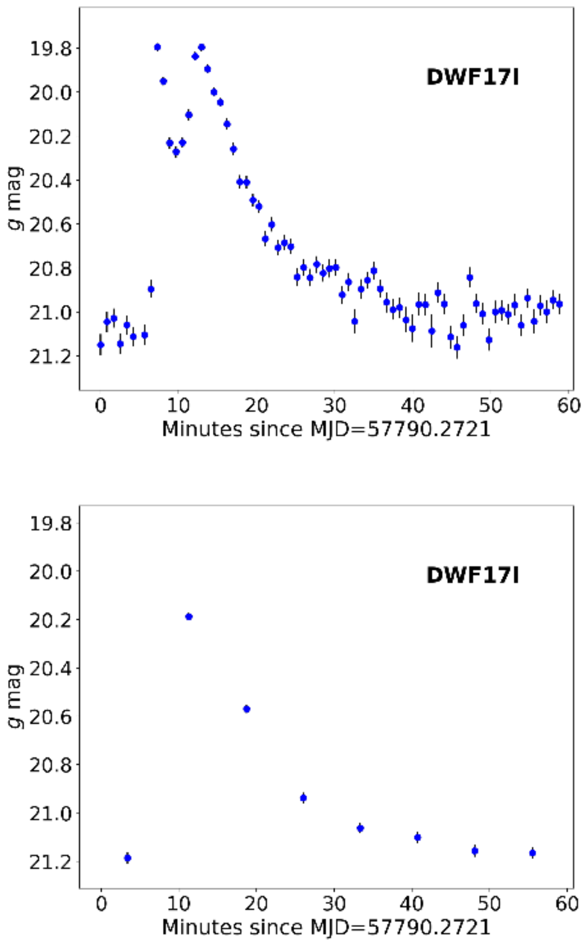

Figure 1. The multi-peak structure of DWF17l is visible in light curves built with series of 20 s exposure images (top panel), but is lost when stacking sets of 9 images (bottom panel). Even if some time resolution is lost, stacking of images acquired during DWF observations allows deeper and more fast-cadenced searches than most existing surveys. The source DWF17l is located at coordinates RA= 6:42:20.333, Dec= –52:10:24.78 (J2000) and the colour of its quiescent counterpart suggests the flare to have arisen from a M5 red-dwarf star.

Table 2. Total time (expressed in hours) for which the target fields were observed.

Date	Target Field				
YYMMDD	3hr	4hr	Prime	FRB131104	Antlia
151218	0.98	1.18	-	-	-
151219	1.21	1.24	-	-	-
151220	1.40	0.91	-	-	-
151221	1.47	1.05	-	-	-
151222	1.66	0.23	-	-	-
170202	-	-	0.97	0.96	0.86
170203	-	-	1.35	0.58	1.00
170205	-	-	1.11	0.87	0.72
170206	-	-	0.96	0.98	1.00
170207	-	-	1.03	1.02	1.02

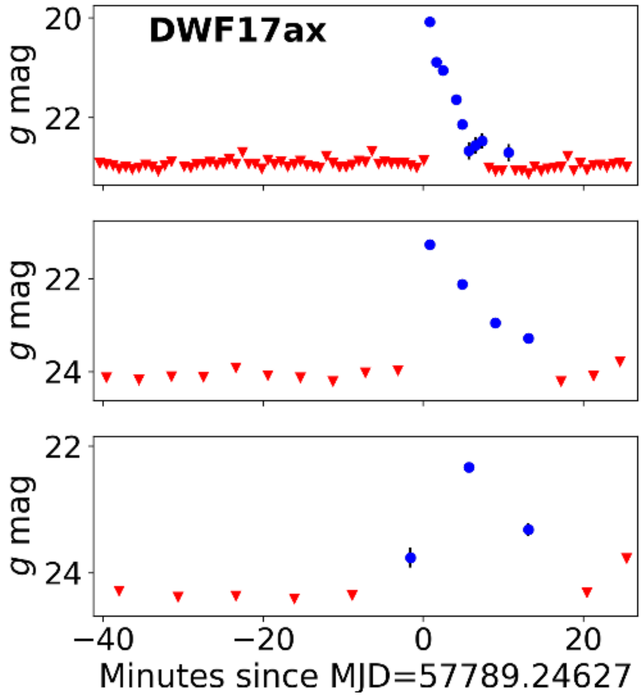

Figure 2. Light curves of the fast-transient candidate labelled DWF17ax (whose discovery images are shown in Figure 3) obtained with individual 20-s exposures (*top*) and by stacking sets of 5 (*centre*) and 9 (*bottom*) fast-cadence images. Red triangles indicate 5σ upper limits.

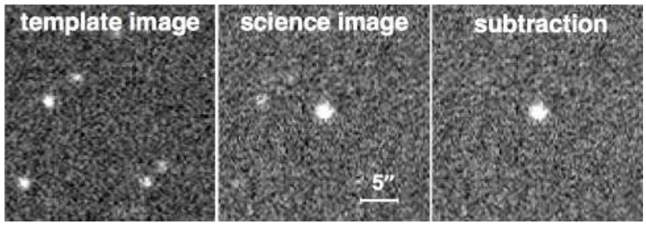

Figure 3. Example of detection 'postage-stamp' images. The extragalactic fast transient candidates (eFTC, in this case DWF17ax) is present in the science image (*center*) and is not present at the same coordinates in the deeper template images (*left*). The image subtraction between science and template images leaves a bright, PSF-shaped residual brighter than the background (*right*). The light curve of DWF17ax is shown in Figure 2.

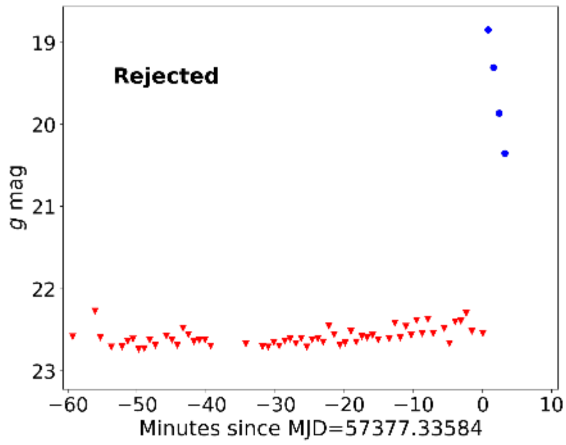

Figure 4. Light curve of an eFTC that did not fulfill the selection criteria described in Section 3. In particular, the candidate was detected in the last image acquired on the observing night in which it was discovered, but we require at least one epoch of non-detection at the beginning and at the end of each observing night to better constrain the transient duration.

University of Technology (now superseded by the OzStar supercomputer).

The *Mary* pipeline automatically outputs a list of candidates and generates three small 'postage stamp' images for each candidate for visual inspection (see for example Figure 3). In addition, a companion code generates aperture photometry light curves centred at the location of the discoveries, with radius 1.5× FWHM measured from nearby stars. Light curves presented in this paper are first calibrated against the all-sky USNO-B1 catalog (which provides a number of Southern-Hemisphere sources large enough to enable calibration of individual CCDs independently) and then calibrated against the AAVSO Photometric All Sky Survey (APASS, Henden et al. 2016) catalogue, that provides AB system measurements. Our tests indicated the g-band magnitudes obtained this way to be consistent with magnitudes from the Sloan Digital Sky Survey catalogue (where there is overlap with DWF fields) within $\lesssim 0.1$ magnitudes.

Template images used for the analysis are always deeper than the individual 20 s exposure images, however their limiting magnitude is usually different for different fields, depending on the availability of archival images from previous observations. For the identification of short-timescale optical transients it is not necessary to have template images older than a few minutes, however the availability of deep templates obtained ad much earlier/later times can greatly help the classification process. When fast transients are identified, we perform a more accurate classification of the detections, based on the photometry performed on deep images, multi-filter information, and object information found when cross-matching with existing catalogues. Asteroids are easily identifiable thanks to the fast cadence of the observations, which makes the movement of the objects in the sky evident when comparing a chronological sequence of images.

First, we search for transient and variable sources in 1870 individual 20s-exposure images, taken with regular cadence. Second, we stack the images in sets of 5, 9, 13, and 17 images to reach deeper magnitude limits and search for fainter fast-evolving transients.

3.1 Selection criteria

At the end of the processing, candidates automatically identified with the *Mary* pipeline are selected aiming at identifying extragalactic fast transient candidates (eFTCs). In particular, we search for astrophysical transient events that evolve at minutes timescales and are not spatially coincident with Galactic sources.

When searching for eFTCs we consider only the first

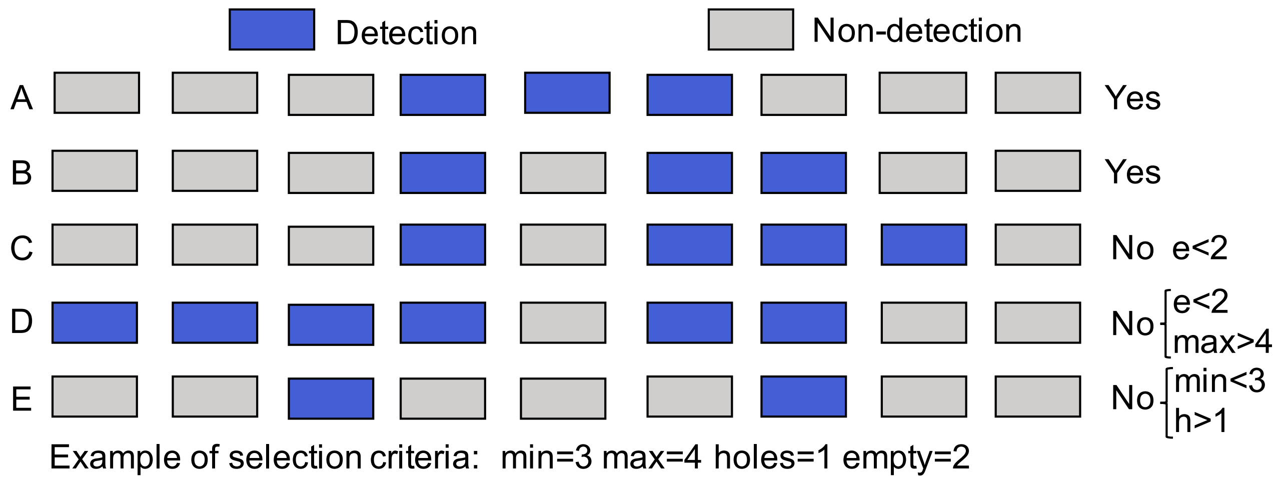

Figure 5. Example of selection criteria application. Given a set of consecutive images (9 images in this example, but on the order of hundred images per night during DWF observations), we define the following selection criteria: at least 3 detections (min=3), at least 2 images without detection at the beginning and at the end of the observing night of that target field (empty=2), at most 4 detections (max=4), and at most 1 image without detection between the first and last detection (holes=1). We apply up to 9 collections of such selection criteria for each set of images in order to keep a nearly constant ratio of minimum number of detections and holes (see Table 3).

night that a detection occurs for those objects detected in more than one night. Upon first detection of a luminosity increase (using image subtraction) at a certain sky location, the pipeline assigns a running ID number to the sky coordinates of the detected object. Consequently, possible re-brightening of the source in the following nights is not given a new ID number and it is not considered among fast-transient candidates presented in this paper.

Our searches returned a large number of candidates ($> 600,000$) most of which are spurious detections, transient/variable objects evolving at long timescales, or Galactic in origin. We reduce the number of spurious detections by requiring candidates to be detected ≥2 consecutive times. Further selection criteria include constraints on the duration of the transients and the rejection of those likely of Galactic origin.

We excluded those events detected at the beginning and/or at the end of each night, constraining the maximum evolution timescales within the time spent on a target field on each night, typically ∼ 1 hr (Table 2). An example of a transient rejected from our sample because it was detected too close to the end of the night is provided in Figure 4.

Searching separately for transients evolving at different timescales (e.g., 2 minutes against 20 minutes full-evolution time) brings several advantages. For example, it enables the rejection of Galactic sources that emit rapid outbursts such as dwarf novae and some active M-dwarfs, favouring the identification of individual minute-timescale bursts. We enhanced the completeness of our searches by allowing the pipeline to 'miss' a number of detections (termed 'holes') between the first and the last detection of a candidate, on the night of first detection. We chose the ratio between the number of holes and the minimum number of detections to be ∼1/3. Table 3 summarises the number of holes that we allowed to be present for each timescale, constrained between the minimum and maximum number of detections. Figure 5 helps visualise the selection criteria on the transient duration.

Table 3. Criteria used for the transient selection. Each row represents a search criterion adopted for each field for each observing night. The first column presents the minimum number of times that a candidate was detected by the *Mary* pipeline; the second column presents the maximum number of images between the first and last detections of each candidate on a given night (extremes included); the third column shows the maximum number of non-detections ('holes') allowed between the first and last detection; the last column indicates the minimum number of 'empty' images, both at the beginning and at the end of each given night, in which the candidate must *not* be detected in order to pass the selection.

min det	max det	holes	empty
2	2	0	1
3	5	1	2
6	8	2	2
9	11	3	2
12	16	4	2
17	23	6	2
24	32	8	2
33	47	12	2
48	64	16	2

As we aim at identifying extragalactic fast transients, we introduced selection criteria to reduce the number of Galactic contaminants (variable and flare stars) in the sample. Using the Source Extractor (SExtractor, Bertin & Arnouts 2010) software on g-band stacks, we exclude those sources with a counterpart detected within a 2.2 arcsec radius with a star/galaxy classification value CLASS_STAR > 0.95. Such a threshold accommodates the change in point spread function (PSF) across the large field of view of DECam and is conservative because it is more likely that stars are classified as galaxies than vice-versa. Thus we can use CLASS_STAR to reduce the number of false positives without significant probability of missing true extragalactic sources, other than QSO.

3.2 Stacking multiple images

In Section 2.3 we explained how we explored a dataset made of a large number of 20 s exposures acquired with regular cadence. The exploration of the shortest timescale dictated by the cadence returns one point in the 3D space defined by timescale, depth, and areal rate (see Figure 6 and Berger et al. 2013b)). Assuming a constant limiting magnitude for each set of images, it is possible to search for transients exploring several timescales, potentially from less than the exposure time up to the duration of the observation of the target field, thus obtaining an array of areal rates that, if well-sampled, defines a broken line in Figure 6.

We enrich the exploration of the parameter space of interest by dividing the images taken on each night in sets of 5, 9, 13, and 17 frames to be stacked together. The larger the number of images stacked together, the deeper we can search and therefore explore a bigger volume of Universe and detect fainter transients. This comes at the cost of reducing the temporal resolution and increasing the timescales of the transients to be discovered, losing information on their evolution, and reducing the effective areal exposure (see Section 6) given the finite total number of images available. The systematic exploration of pairs of timescale and limiting magnitudes defines a surface in Figure 6.

The criteria to select eFTCs in series of stacked images are the same as described in Section 3.1 and in Figure 3, with the sole difference that the minimum number of 'empty' stacked images, both at the beginning and at the end of each given night, in which the candidate must not be detected in order to pass the selection is always equal to 1. The choice of the number of images to stack (1, 5, 9, 13, 17) and the type of stacking (median) are dictated by technical reasons. Stacking more than 17 images together would cause the analysis to be meaningless in several cases, as no transient would possibly meet the criteria for the selection. We found that considering steps of 4 images balances well the need to densely sample the exploration space and the availability of computational resources, highly demanded when running the pipelines on thousands of images. Moreover, stacking an odd number of images is particularly suitable for median-stacking. The limitation to stack images considering median values derives from the structure of the *Mary* pipeline used to perform the analysis, which lacks a cosmic ray-rejection module that reduces the number of false positives when stacking a large number of images using averaging. In fact, average-stacking would have allowed us to be more sensitive to bright events with very short duration, thus we acknowledge that average-stacking would have been the preferred choice to adopt in this work. We are planning to adopt average-stacking in future work. Nevertheless, median-stacking images allowed us to achieve excellent results.

4 RESULTS

In order to carry out the searches described in Section 3, we ran the *Mary* pipeline 2744 times in total, each time processing 59 CCDs in parallel. The analysis of our dataset

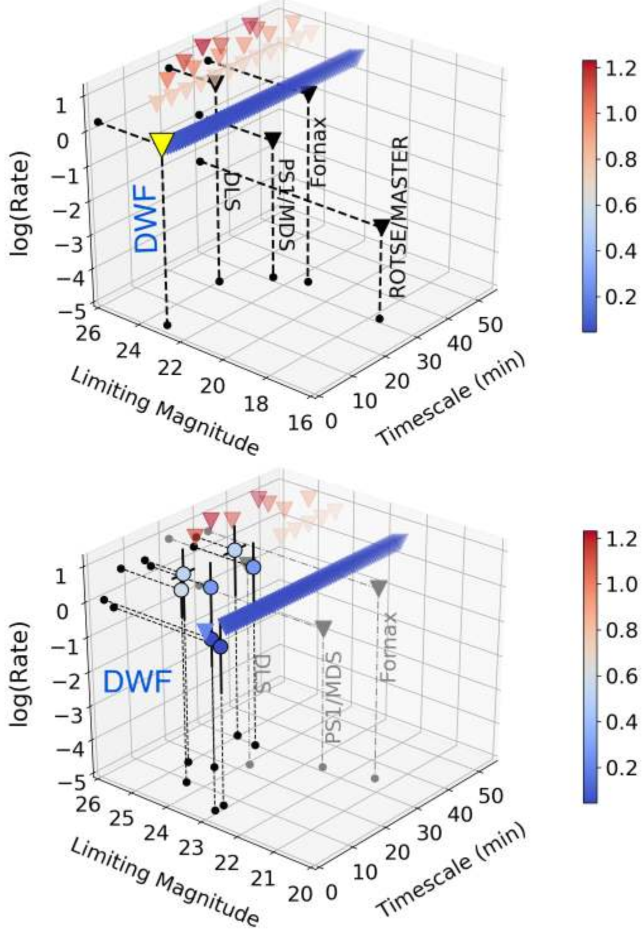

Figure 6. Plot of the new phase-space region explored, where rates of extragalactic fast transients ($\mathrm{deg}^{-2}\mathrm{day}^{-1}$) are plotted at each combination of limiting magnitude (i.e., depth) and timescale (expressed in minutes). The colour-map also represents the logarithm of the rates and helps visualising the differences between different points. *Top* – Triangles indicate upper limits placed during the systematic exploration of the DWF data set presented in this paper, assuming that all the eFTCs that passed our selection criteria are Galactic or spurious detections. The stacking of sets of images allows the exploration of different depth regimes, thus our results approximately describe a surface in the limiting magnitude – timescale – transient rates phase-space. The yellow triangle represents the shortest timescale that we can explore (τ = 1.17 min), for which we obtain $R_{eFT} < 1.625\,\mathrm{deg}^{-2}\mathrm{day}^{-1}$. Black triangles indicate upper limits for past surveys, here presented as in Berger et al. (2013b). *Bottom* – Same plot as the top panel, but assuming that those 4 eFTCs that we cannot confidently classify as Galactic are, in fact, extragalactic in nature. This scenario is optimistic and upper limits presented in the top panel represent a more conservative result of this work.

returned 318 672 candidates[5], including thousands of real variable and transient sources along with a large number of false positives. We reduced the number of candidates to $\sim 10,000$ by applying the selection criteria on the duration of the transients, presented in Table 3. All candidates were

[5] This number includes possible repetitions of the same candidate when stacking different sets of multiple images.

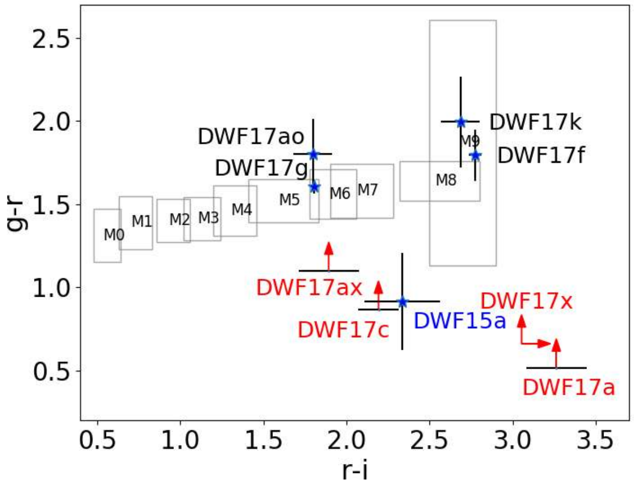

Figure 7. Colour-colour plot showing measurements of possible counterparts to the eFTCs listed in Table 4. Magnitude values were calibrated using the APASS catalogue. Boxes frame regions of the colour-colour plot where different types of M-dwarfs lie (West et al. 2011).

visually inspected at this preliminary stage and further inspection was performed after applying the following cuts.

When all the selection process described in Section 3.1 was completed, 1846 candidates remained. Visual inspection of those candidates, exclusion of asteroids, and the removal of repetitions due to the detection of the same object when stacking different sets of images left us with 25 candidates. Of those 25 candidates, we classified one as AGN activity, 2 were already catalogued as variable stars in the Vizier database[6], and 13 have parallax or high proper-motion measurements reported in the second *Gaia* Data Release (Gaia Collaboration et al. 2016, 2018). Excluding those Galactic and nuclear sources from our sample, 9 eFTCs constitute our short list. Their identifications and sky coordinates are presented in Table 4. We stress that many more real transient sources were identified than those reported in this paper, however a limited number of those passed the selection criteria that we established.

We further investigate the 9 short-listed eFTCs using SExtractor CLASS_STAR on deep stacks in *riz* bands (where available), colour information, and behaviour of their light curves. Results of the multi-band S/G classification are presented in Table 5. Five eFTCs (DWF15a, DWF17a, DWF17c, DWF17f, and DWF17g) can be classified as stellar if we consider again a S/G threshold CLASS_STAR > 0.95. Colours are obtained with photometric measurements on deep stacks of images acquired before the transient detection. Magnitudes are calibrated using the AAVSO Photometric All Sky Survey (APASS, Henden et al. 2016) catalogue. Sources with a detectable counterpart in deep stacks and in different filters are plotted in Figure 7 (see also Table 4). We also attempt a comparison between our data with flare star models computed from *Kepler* observations (Davenport et al. 2014). One example of such a comparison is presented in Figure 10 for the eFTC candidate DWF17a. Specific cases are discussed below:

- DWF15a – Possibly stellar based on its i-band S/G classification. However, faint detections in deep stacks place it outside the M-dwarf stripe in the $g-r, r-i$ colour plot. The light curve is consistent with a template flare star light curve (Figure 10).
- DWF17a – Most likely a stellar flare based on the multi-band S/G classification. The light curve evolves faster than the stellar flare model (Davenport et al. 2014) shown in (Figure 10) We note that a large difference $r-i > 3$ suggests the flare to be generated from a star of type later than M9.
- DWF17c, DWF17f – Most likely stellar flares based on the multi-band S/G classification (CLASS_STAR > 0.95 in at least two bands). The light curves compare well with the stellar flare model. These sources can be classified as M7 (DWF17c) and M8-M9 (DWF17f) stellar flares.
- DWF17g – Very likely M5-M6 star flare.
- DWF17k – The S/G classifier suggests the object to be non-stellar in r and i band, where the object is detected with a signal-to-noise ratio S/N∼10. However, Figure 11 shows that S/G values for sources in the field where DWF17k is located, the FRB131104 field, are distributed more towards non-stellar classification than the Prime field, chosen for comparison, despite the latter being located at higher Galactic latitude. The location in the colour-colour plot suggests DWF17k would be a M8-M9 star flare. A Galactic nature of this source is also supported by a good resemblance between the light curve and the template stellar flare we consider. However, the information in hand does not allow us to conclude that this source is stellar.
- DWF17x – As for DWF17k, the S/G classification may be biased toward non-stellar objects in the field where DWF17x is located. Thus both the S/G classification and the upper limits in the colour-colour plot in Figure 7 give little information about the nature of DWF17x. The light curve matches well the flare-star model (Figure 10). The small discrepacy could be due to the wrong choice of the peak time, that a higher cadence would have improved. We cannot conclude that this source is either Galactic or extragalactic.
- DWF17ao – The S/G classification suggests a non-stellar origin for DWF17ao, which could be due to the relatively large PSF of the Prime field deep stacks (seeing $\sim 1.5''$). On the contrary, the multi-peak light curve advocates for a flare star event that, according to the colour-colour plot in Figure 7, may have a M5-M6 star progenitor. More information is required to confidently classify this object.
- DWF17ax – The S/G classification suggests an extragalactic origin for this candidate, with the same caveats about the seeing described for DWF17ao. The fast-cadence light curve of DWF17ax (Figure 2, top-left panel) shows a possible multi-peak structure, common among flare stars. If the transient is indeed a flare star, its progenitor's class could range between M5 and M7. As for DWF17k, DWF17x, and DWF17ao, the information available is not conclusive about the nature of this object.

[6] https://vizier.u-strasbg.fr/viz-bin/VizieR

Table 4. Identification name, target field, and coordinates of those fast-transient candidates that passed our selection criteria. The magnitude variation is computed as the difference between the deepest g-band measurement available and the observed peak magnitude, therefore the actual variation in magnitude is likely larger than what is reported here. The light curves of the eFTC presented here are shown in Figure 2 and in Figures 8-9. Candidates in the lower half of the table, below the horizontal line, are those for which the multi-band S/G classifier cannot determine whether the quiescent counterpart to the transients is stellar.

ID	Field	RA	Dec	$-\Delta g$	g	r	i	z
DWF15a	4hr	4:11:05.702	−55:40:17.87	∼ 5.0	24.78 ± 0.20	23.86 ± 0.21	21.53 ± 0.08	-
DWF17a	Antlia	10:25:53.642	−35:31:20.67	>2.4	>24.15	23.64 ± 0.18	20.37 ± 0.01	19.90 ± 0.023
DWF17c	Antlia	10:28:48.603	−36:07:00.54	>2.4	>24.15	23.29 ± 0.12	21.09 ± 0.02	20.97 ± 0.07
DWF17f	Antlia	10:27:36.287	−35:36:59.79	1.8	23.53 ± 0.15	21.74 ± 0.04	18.96 ± 0.01	18.97 ± 0.01
DWF17g	Antlia	10:25:47.560	−35:41:54.92	0.8	21.61 ± 0.04	20.00 ± 0.01	18.198 ± 0.003	17.990 ± 0.005
DWF17k	FRB131104	6:47:05.788	−51:27:38.88	∼4.8	25.19 ± 0.25	23.19 ± 0.11	20.50 ± 0.07	-
DWF17x	FRB131104	6:45:04.601	−51:38:18.26	>4.6	>25.0	>24.3	21.29 ± 0.26	-
DWF17ao	Prime	5:52:29.591	−60:49:50.92	3.6	25.46 ± 0.18	23.66 ± 0.10	21.86 ± 0.05	21.16 ± 0.01
DWF17ax	Prime	5:59:00.662	−62:02:11.03	>5.6	>25.6	24.53 ± 0.16	22.64 ± 0.09	21.98 ± 0.02

Table 5. SExtractor star/galaxy classification of short-listed eFTCs in quiescence in deep images. The last column indicates whether the sources were classified as stellar with score S/G > 0.95 in at least one band. In such cases, we consider the SExtractor classification to be in support of the eFTCs being Galactic stellar flares.

ID	S/G g	S/G r	S/G i	S/G z	S
DWF15a	0.591	0.221	0.966	None	Y
DWF17a	None	0.005	0.983	0.973	Y
DWF17c	None	0.743	0.98	0.963	Y
DWF17f	0.55	0.98	0.986	0.986	Y
DWF17g	0.717	0.979	0.983	0.984	Y
DWF17k	0.038	0.0	0.035	-	N
DWF17x	None	0.557	0.356	-	N
DWF17ao	0.0	0.832	0.667	0.852	N
DWF17ax	None	0.001	0.0	0.331	N

5 SEARCHES FOR MULTI-WAVELENGTH COUNTERPARTS

The DWF programme coordinates simultaneous multi-wavelength observations of the target fields. Moreover, we take templates using the wide-field SkyMapper telescope weeks before DWF observing runs and we use it to perform interleaved, nightly observations during DWF, and late-time regularly-cadenced observations weeks after DWF to characterise long-duration transients. In this section we present searches for gamma-ray and radio signals possibly associated with the 4 most promising eFTCs among those presented in Section 4 using the Parkes, Molonglo, *Swift*, and *Fermi* observaotries. Details and results of these searches are summarised in Table 6. Searches for long-duration optical transient counterparts with SkyMapper are described in Section 5.3.

5.1 Searches for gamma-ray signals

We explore data acquired with *Fermi* and *Swift* gamma-ray telescopes at times close to the last non-detection of our selected eFTC.

Neil Gehrels Swift Observatory

Observations with the *Neil Gehrels Swift Observatory* (hereafter *Swift*) were performed under approved Cycle 11 and Cycle 13 programmes (PI Pritchard). Moreover, the large FoV of *Swift*/Burst Alert Telescope (BAT, Barthelmy et al. 2005) allowed DWF target fields to be observed even when the satellite was pointing at other scientific programme targets with its narrower-field instruments X-ray Telescope (XRT) and UltraViolet/Optical Telescope (UVOT). The *Swift* team smartly scheduled *Swift* observations of other science programmes to maximise the observability of DWF fields with BAT. We searched for gamma-ray counterparts to five most promising eFTCs: DWF15a, DWF17k, DWF17x, DWF17ao, DWF17ax. Some of the DWF *Swift* time had BAT, XRT, and UVOT on the target fields. However, none of the sources were located within the FoV of the XRT and UVOT, therefore we limit our analysis to the BAT data.

We considered the last optical non-detection as onset time (T0). Onset times are listed in Table 6. We expect T0 to be accurate within 30 s from the actual onset of the eFTCs because of the short rise-time of the transients and the high cadence of our observations. The nature of the eFTCs being uncertain, we explored a conservative time window of ±1800 s around T0, larger than the evolution timescale of the candidates. Except DWF17ao, all candidates were located in the BAT FoV for some period of time within the search interval. DWF17ao occurred when *Swift* was in safehold, so no data were available. A wider temporal search (years before and after the events) is planned for future work.

When trying to identify gamma-ray counterparts, unconstrained by physical models, we searched:

- The raw light curves, to see if there are any obvious GRB-like structures around T0. We did not find GRB-like events in raw light curves.
- The available event data, from which we can make a background-subtracted (i.e., mask-weighted) light curve using the source location. In particular, we looked for astrophysical signals in mask-weighted light curves (e.g., burst-like features or some continuous time bins with count rate above $\sim 3\sigma$). We also created images of the available event data interval and search for any detections at the source location. No source was found above 3σ significance.
- The BAT survey data, which consisted of continuous data binned in 300 s bins. Again, no signal was detected at the source locations at $> 3\sigma$ significance.

In summary, no significant ($\gtrsim 3\sigma$) gamma-ray source was found when searching in BAT raw data, BAT event

Table 6. This table indicates when gamma-ray and radio telescopes were observing the region of sky where a subset of eFTCs (Table 4) were discovered. The onset time indicated represents the MJD of the last non-detection of the eFTC. We looked into *Swift*/BAT data to identify gamma-ray counterparts, and we used the Parkes and Molonglo radio telescopes to search for FRBs. We coordinated *Swift*, Parkes, and Molonglo to observe fields simultaneously with DECam as part of the DWF programme. In addition, we looked for gamma-ray triggers issued by the *Fermi* satellite ±1 day from the onset time, with the caveat that the location where the eFTC was detected may have been outside the *Fermi* field of view for part of the time.

ID	Onset (MJD)	*Fermi* (days)	*Swift*/BAT (minutes)	Parkes (minutes)	Molonglo (minutes)	Gamma-ray detections	FRB detections
DWF17k	57789.27229	+/- 1	+8 +30	−5 +60	−8 +65	0	0
DWF17x	57786.29119	+/- 1	−10 −3; +3 +27	−25 +45	-	0	0
DWF17ao	57790.24767	+/- 1	-	−45 +35	−2 + 25	0	0
DWF17ax	57789.24627	+/- 1	−30 −18	−20 +30	−47 + 12	0	0

data, and BAT survey data within T0 ± 1800 s, where T0 is the onset time. More precise time slots in which the selected eFTCs were in the BAT FoV are reported in Table 6.

Fermi

We searched for GRB counterparts detected by the *Fermi* Gamma-ray Burst Monitor (GBM, Meegan et al. 2009) during the optical transients presented in this work. The GBM is composed of 12 sodium iodide (NaI) and two bismuth germanate (BGO) scintillation detectors, covering respectively the energy range 8 keV-1 MeV and 200 keV-40 MeV, with a field of view > 8 sr. We searched for counterparts in the Fermi GBM Burst Catalog [7], that lists all triggers observed that have been classified as GRBs. For completeness, we also searched in the *Fermi* GBM Trigger Catalog[8], that lists all triggers (even not classified as GRBs) observed by one or more of the 14 GBM detectors, and also in the Subthreshold Catalog[9].

Table 6 reports the results of the research in the catalogues, with a time window of +/− 1 day from the onset of the optical transient. No gamma-ray sources were found spatially and temporally coincident with the 10 optical transient reported in Table 4. However, we found three transients, DWF17c, DWF17f and DWF17g, spatially located within the 3σ contour plot of the GBM localization of a GRB (GRB170208). This GBM event occurred on 2017-02-08 at 18:11:16.397, more than 1 day after the optical transients, and is separated by more than 10 degrees from the positions of the optical transients. Due to the time-lag between the optical and gamma-ray events and to the poor localization of the GBM detectors, we conclude that GRB170208 cannot be the counterpart to DWF17c, DWF17f or DWF17g.

5.2 Searches for coincident fast radio bursts

Parkes – as part of the SUrvey for Pulsars and Extragalactic Radio Bursts (SUPERB) (Keane et al. 2018), we explore the data acquired using the 21-cm multibeam receiver (Staveley-Smith et al. 1996) deployed on the Parkes radio telescope. The FWHM of each of the 13 beams is ∼ 14 arcmin, with an areal ∼ 2σ 13-beam coverage of ∼ 3 deg^2.

The output of each beam is processed by the Berkeley-Parkes-Swinburne Recorder (BPSR) mode of the HI-Pulsar (HIPSR) system (Keith et al. 2010; Price et al. 2016; Keane & Petroff 2015). The BPSR produces 8-bit, Stokes-I filterbanks with spectral and temporal resolution of 390.625 kHz and 64 µs respectively, over 1182–1152 MHz (340 MHz bandwidth). Searches for FRBs in the filterbanks are performed in real time using the dedicated GPU-based single pulse search software, HEIMDALL[10]. Candidate selection criteria are listed in §3.3.2 of Keane et al. (2018). No FRBs were detected in real-time with S/N ≥ 10. A more thorough offline processing of the data with a lower S/N threshold of 6 did not yield any significant FRB detections either.

Molonglo – the Molonglo radio telescope, a Mills-cross design interferometer located near Canberra, Australia, is a pulsar timing and FRB detection facility (Bailes et al. 2017). Molonglo is sensitive to right-hand circularly polarised radiation, and operates in the spectral range of 820-850 MHz. The relatively large (≈ 4 deg ×2.8 deg) primary beam of Molonglo is tiled with 352 thin synthesised 'fanbeams' that overlap at their FWHM (≈ 45 arcsec). The output of each fanbeam is an 8-bit filterbank with spectral and temporal resolution of 98 kHz and 327 µs respectively. These filterbanks are searched for FRBs using a modified version of HEIMDALL, and burst candidates are validated via a machine learning pipeline operating in real-time (Farah et al. 2018, Farah et al. in preparation). We search for FRBs with widths in the range 327 µs to 42 ms, dispersion measures (DMs) in the range 0 <DM< 5000 pc cm^{-3}.

Both facilities were observing the region of sky where the selected eFTC were discovered, and the results are summarised in Table 6. No FRBs were detected during the observations.

5.3 Optical interleaved and long-term follow-up

We obtain photometry from the SkyMapper 1.35m telescope located at Siding Spring Observatory in New South Wales, Australia (Keller et al. 2007). We have established a follow-up programme which coordinates with the DWF

[7] https://heasarc.gsfc.nasa.gov/W3Browse/fermi/fermigbrst.html
[8] https://heasarc.gsfc.nasa.gov/W3Browse/fermi/fermigtrig.html
[9] https://gcn.gsfc.nasa.gov/fermi_gbm_subthresh_archive.html
[10] https://sourceforge.net/projects/heimdall-astro/

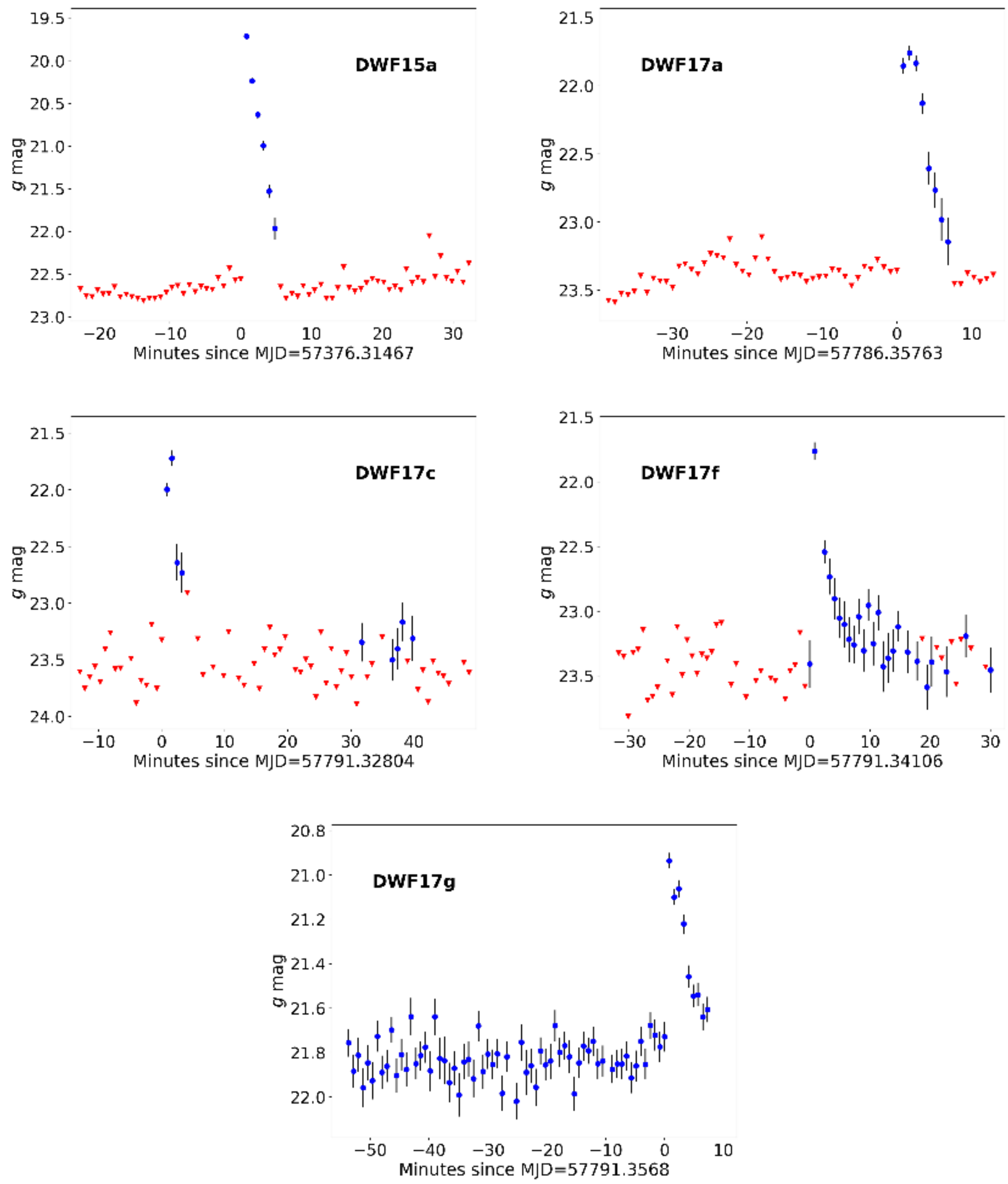

Figure 8. Light curves of selected extragalactic fast-transient candidates (eFTCs) that we classify as stellar flares based on the multi-band S/G separation (Table 5). Red triangles represent 5σ forced-photometry upper limits. Candidates DWF17f and DWF17g show measurements on the last epochs of the observing sequence, missed by the image-subtraction pipeline with threshold at $\sim 7\sigma$ significance. Details about these sources are presented in Table 4.

programme to obtain interleaved nightly observations during DWF (hours-later observations once it becomes night in Australia), and late-time regularly-cadenced observations weeks after DWF to characterise long-duration transients and those that can be associated with fast transients, such as supernova shock breakouts. We obtain 100 s exposures in *gr* bands centred on each DWF field, which are covered by the wide-field of view of SkyMapper (5.7 deg^2) when weather is suitable. Whenever possible, we obtain template images prior to the DWF run. We use the SkyMapper Transient Survey Pipeline (Scalzo et al. 2017) to detect transients and obtain subtracted photometry when possible. In addition to these images, we obtain photometry from the SkyMapper Supernova Survey (Scalzo et al. 2017) and the Southern Sky Survey (Wolf et al. 2018) when available for the candidates discussed in this work. These images are used to check for long term variability and are available in the *uvgriz* passbands up to magnitudes $i = 20.27, z = 19.42, u = 19.34, v = 19.59, g = 21.57, r = 21.25$ depending on the coverage of the source. Long term variability is verified from March 2016 to June 2018 for DWF17a, DWF17c, DWF17f, DWF17g and

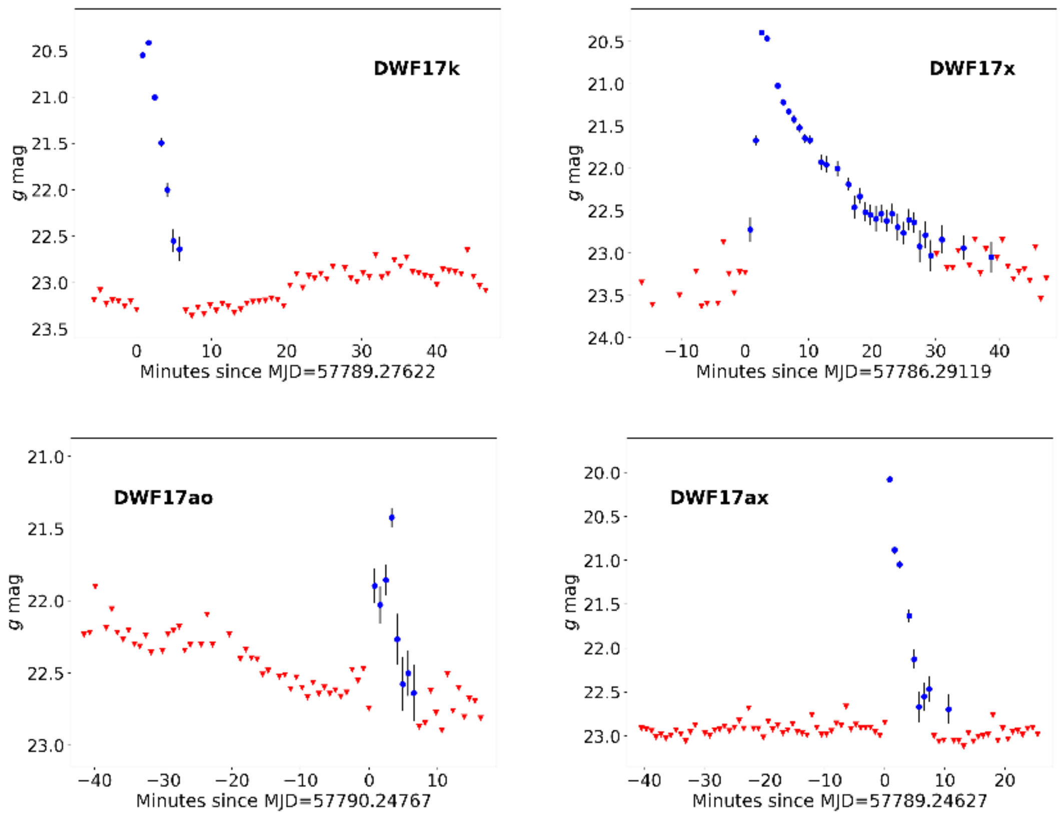

Figure 9. Light curves of selected extragalactic fast-transient candidates (eFTCs) that we cannot classify as stellar flares based on the information available. Details about the eFTCs are presented in Table 4. The light curve of DWF17ax can be found also in Figure 2, where we show the effect of image stacking on a transient light curve.

up to March 2017 for DWF17k, DWF17x and up to August 2018 for DWF17ao and DWF17ax (see Appendix B).

In this search for an optical counterpart to the fast transient candidates, there are no sources at the location of the DWF transients except for two cases, DWG17f and DWF17g. DWF17f was detected in the z filter on March 26th 2016 with magnitude 19.1 ± 0.1. DWF17g was detected more than once with SkyMapper in the gr bands on February 22nd and 27th and z band on March 26 but we do not see any significant variability in any of the observations ($g = 21.0, r = 20.2, z = 19.1$).

6 RATES OF EXTRAGALACTIC FAST OPTICAL TRANSIENTS

Under the assumption that all the minute-timescale transients that we detected are of Galactic nature, we can estimate upper limits to the rates for extragalactic fast optical transients. We follow the same procedure presented in Berger et al. (2013b) in order to enrich and extend the results that they obtained. The rate of extragalactic fast transients is defined as:

$$R_{eFT} = N/(e_\tau * E_A) \quad (1)$$

where N is the number of transient events (here, $N = 3$ is defined for a non-detection, 95% confidence), e_τ is the detection efficiency for the chosen timescale, E_A is the effective areal exposure, defined as:

$$E_A = \mathrm{FoV_{eff}} * (n_{\mathrm{im,tot}}/n_{\mathrm{im,set}}) * \tau \quad (2)$$

where $\mathrm{FoV_{eff}}$ is the effective field of view explored, $n_{\mathrm{im,tot}}$ is the total number of images, $n_{\mathrm{im,set}}$ is the number of images constituting the smallest set that allows exploration of the chosen timescale, and τ is the evolution timescale of the transient. In this work we analysed 25.76 hr of data, over 10 half-nights. We searched for transients over an effective area of $\sim 2.52\,\mathrm{deg}^2$ per pointing. The efficiency of the detection

Table 7. Rates calculated assuming that the 4 unclassified eFTCs (DWF17k, DWF17x, DWF17ao, and DWF17ax) are indeed extragalactic fast transients. Such an assumption is optimistic and it is more likely that the transients are Galactic cool star flares. Rates reported here are also plotted in Figure 6. Poissonian lower and upper limits for the rates (95% confidence) are taken from tables in Gehrels (1986).

timescale (minutes)	Lim. mag	Rate ($\mathrm{deg}^{-2}\mathrm{d}^{-1}$)	Lower ($\mathrm{deg}^{-2}\mathrm{d}^{-1}$)	Upper ($\mathrm{deg}^{-2}\mathrm{d}^{-1}$)
2.83±0.33	23.0	0.86	0.15	2.72
5.33±0.33	23.0	0.40	0.02	1.90
7.83±1.67	24.3	3.85	0.68	12.12
16.17±1.67	24.3	1.87	0.10	8.85
28.67±1.67	24.3	1.84	0.09	8.73
14.50±3.00	24.9	3.27	0.17	15.51
29.50±3.00	24.9	3.21	0.16	15.23

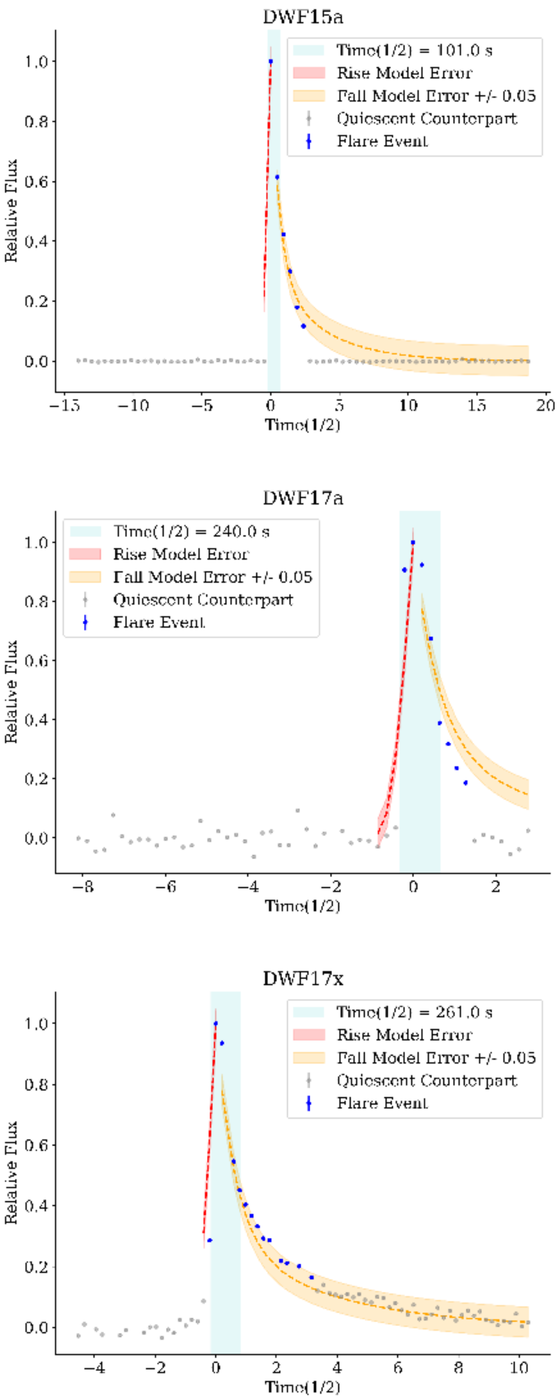

Figure 10. Flare-star model for the eFTC DWF15a (top), DWF17a (centre), and DWF17x (bottom). Data are compared with template white light flares based on *Kepler* observations (Davenport et al. 2014), where Time(1/2) is the FWHM of the flare. When no permanent source is detectable in fast-cadenced g-band images outside the flare times, we simulate a Gaussian distribution of data points centered on the magnitude value (or upper limit) calculated on deep stacks (see Table 4). We normalised the flux to the brightest point of the light curve, however the peak of the flare is likely brighter and shifted in time by $0 \lesssim t_{\rm peak} \lesssim 30$ s, given the cadence of our observations. A better guess of time and flux of the peak would likely result in a better fit of the model to the light curves in some cases, but poorer in others.

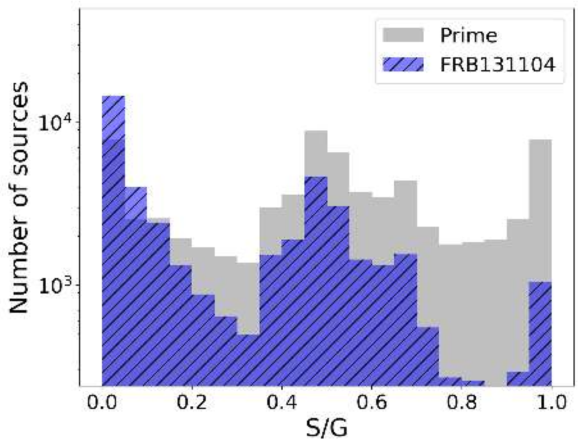

Figure 11. Distribution of star/galaxy classification for sources present in the central part of the FRB131104 and Prime target fields, imaged in DECam i-band. The depth of the images is i <23.67 for FRB131104, i <24.04 for Prime. Sources in the FRB131104 field are biased towards low S/G values probably due to poorer observing conditions (seeing $\sim 1.7''$ for FRB131104 against $\sim 1.5''$ for Prime).

pipeline is based on the test results described in Andreoni et al. (2017), that returned 96.7% completeness matching two consecutive epochs at S/N>10. Thus we can assume $e_\tau = 0.967$ for the exploration of the shortest timescale, where 2 (and only 2) detections must occur in consecutive images. The completeness rapidly reaches > 99.9% for the exploration of longer timescales thanks to the fact that a transient is selected even if 'missed' in $\sim 1/3$ of the images that lie between the first and the last detection of the event on the first night it was detected (with first and last images included in the count).

The shortest timescale that we can explore is τ = 1.17 min, or 1 min 10 s, considering 20 s exposures interleaved by 30s off-sky time. We obtain $E_A = 1.91\,\mathrm{deg}^2\mathrm{day}$ and an upper limit for the areal rate of $R_{eFT} < 1.625\,\mathrm{deg}^{-2}\mathrm{day}^{-1}$, represented with a yellow marker in Figure 6. The results for every combination of timescale and depth are plotted in Figure 6 and presented in Appendix A. Results of past surveys are summarised in Berger et al. (2013b) and include the Pan-STARRS1 Medium-Deep Survey (PS1/MDS Berger et al. 2013b), the Deep Lens Survey (DLS, Becker et al. 2004), the survey of the Fornax galaxy cluster (Rau et al. 2008), ROTSE III (Rykoff et al. 2005), and MASTER (Lipunov et al. 2007). In Figure 6 we consider first the case in which all the selected eFTCs are Galactic in nature or spurious detections. This is the most probable scenario, given that our inability to classify those eFTCs may derive from observational limitations (see Section 4). Secondly, we plot rates for extragalactic fast transients on the assumption that DWF17k, DWF17x, DWF17ao, and DWF17ax are extragalactic (see also Table 7). Uncertainties on the rates were taken from Gehrels (1986) using Poissonian statistics and 95% confidence. Uncertainties on the timescales are given by the cadence at which those eFTCs were discovered (usu-

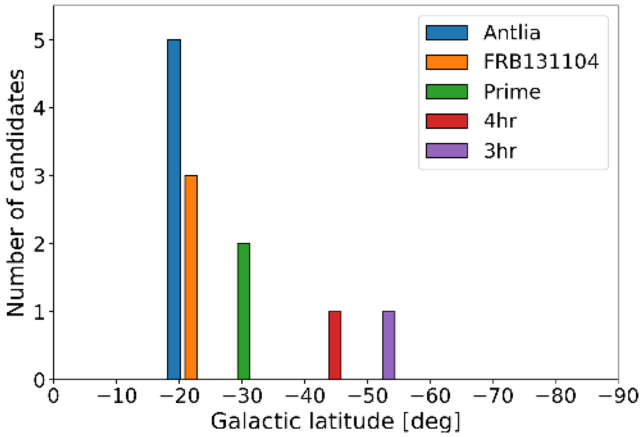

Figure 12. The number of eFTCs in Table 4 plotted against Galactic latitude, expressed in degrees. The bars of the histogram are 2° wide. The increase in the number of eFTCs in the Antlia field may be higher than expected as a result of the lower Galactic latitude (when extrapolating to zero latitude), or may indicate detection of extragalactic fast transients, given the proximity of the galaxy cluster. However, we caution that the sample is too small for any definitive result.

ally more than one) and by the duration selection criteria (Table 3).

7 DISCUSSION

This work probed the minute-timescale transient sky with deep and fast-cadenced optical observations. Such a region of the timescale-depth phase-space is accessible with only a few existing facilities and no search with the combination of area, depth, and fast cadence of DWF has ever been performed. Our searches unveiled hundreds of transient and variable events, many of which evolve in minutes. Out of a short list of 9 eFTCs that passed our specific extragalactic fast transient selection criteria, 4 may be bona-fide extragalactic transients evolving on timescales of minutes.

Our selection criteria helped reduce contamination from Galactic sources and from transients (Galactic or extragalactic) evolving at timescales longer than ∼ 1 hr. On the other hand, we are heavily biased toward discovering flare stars by imposing such strict temporal constraints. In particular, we expect to detect 'strong' flares from distant ($\gtrsim$ 2 kpc), late-type M-dwarfs difficult to detect when quiescent, as these would pass our non-stellar criteria for extragalactic events using our stellarity classifier. Our results (see Section 4) suggest those expectations to be correct, as most of the selected eFTCs are likely associated with late-type (usually ≥ M6) stars.

Although no deep spectra of the eFTCs exist, their peak and quiescent magnitudes and short evolution duration provide some limits on their nature when compared to known transients. The quiescent colours and magnitudes of DWF17k, DWF17x, DWF17ao, and DWF17ax are consistent (or roughly consistent) with an M9, M9/L, M5/M6, and M6 star at ∼ 100 pc, < 100 pc, 1000–1500 pc, and 850–1200 pc, respectively, and are thus thought to be flare stars. However, their star/galaxy classifications are inconsistent with stellar profiles. If the quiescent objects are, instead, host galaxies, their colours are inconsistent with star forming and other galaxy templates, but could be reddened elliptical or E+S0 galaxies, luminous infrared galaxies (LIRGs), or similar at z ∼0.5–1.5, depending on galaxy type. The quiescent magnitudes are too bright for host galaxies at $z > 2$, placing them on the bright tip of the galaxy luminosity functions (M ∼ −23 and brighter) before extinction correction.

If the eFTCs are considered as fast nova-like bursts (M ∼ −8 to −9), their host galaxies are constrained to M ∼ −5 to −9 compact dwarf galaxies or globular clusters at ∼ 4–11 Mpc. If considered as supernova shock breakouts (M $\gtrsim$ −20 adopted here), the hosts are constrained to z <0.25–0.4 and the late-time photometric limits requires any associated supernova to fainter than M ∼ −14 to −19 at ∼100 Mpc to z ∼ 0.3, respectively. The quiescent colours are inconsistent with essentially all galaxy types in this redshift range, unless heavily reddened. Finally, if the eFTCs are optical counterparts to GRBs, the quiescent colours and magnitudes are roughly consistent with M ∼ −21 to −23 reddened host galaxies at z ∼ 0.5–1.5 and optical afterglows of M ∼ −22 to −23 before host or event extinction corrections.

During searches for extragalactic fast transients, hostless candidates may be excluded because their light curves resemble flare-star light curves. To test the validity of such an argument, we compared the template flare-star model (described in Section 4) with the light curve of the prompt optical flash that accompanied GRB 110205A at redshift $z = 2.22$ (Cucchiara et al. 2011). The flash remained visible for less than 15 minutes, providing a good example for the type of fast transient that this work targeted. Figure 13 shows that, even without applying any re-scaling of the light curve at lower or higher redshift, the white light data points are consistent with the flare-star template. This comparison suggests that the lack of a bright host galaxy and light curve information alone cannot exclude the extragalactic nature of a fast transient candidate.

The distribution of eFTCs over Galactic latitude (Figure 12) provides further indication that most of our eFTCs are Galactic flare stars, as they appear to be more common as the target fields approach the Galactic plane. A strong caveat is that Antlia is the field located at the lowest Galactic latitude among the fields considered in this analysis, but also includes the nearby Antlia galaxy cluster, which is at a comoving distance of ∼41 Mpc. Therefore our observations cannot yet exclude that minute-timescale fast optical transients are detectable with deep, fast-cadence observations both in our Galaxy and in the outskirts of nearby galaxies. The dependence of the number of eFTCs on Galactic latitude seems consistent with targeted flare-star population studies (e.g., Kowalski et al. 2009). We refrain from further quantifying such dependence because of the small number of eFTCs reported in this paper, leaving it as the primary subject of a separate on-going analysis.

Finally, light curves of confirmed stellar flares show diverse behaviour, usually made more complex by a series of flares occurring in short time frames. High time sampling can help understand the physics of flare stars and improve temporal morphology studies. Flaring events such as the double-peak event in Figure 1 show that poor cadence can lead to misleading interpretation of parameters such as the flare duration, without accounting for the presence of multi-

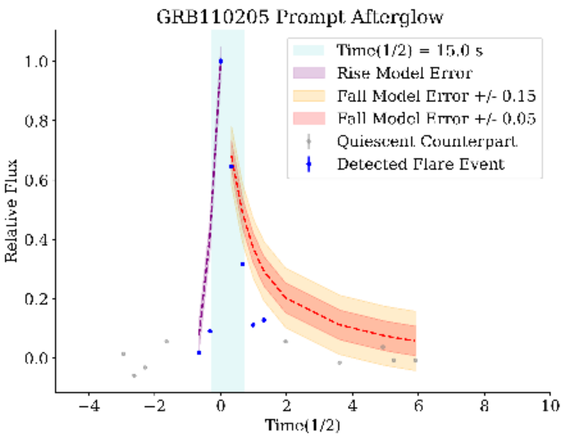

Figure 13. Observations of the optical flash associated with GRB110205A (Cucchiara et al. 2011) are compared with the Davenport et al. (2014) flare star model described in Section 4 and Figure 10.

ple peaks. In addition, fit-to-peak estimates of peak luminosity and released energy can be overestimated using simple power-law fits. Such overestimation can affect the study of flares individually as well as a population, while underestimating the complexity of the flaring activity. Deep imaging and fast time sampling are necessary to compute quantities such as the duration and peak luminosity of the flares. Future work (Webb et al., in preparation) will include detailed and complete studies of hundreds of flare stars identified during the analysis presented in this work.

8 SUMMARY

In this paper we analysed part of the all-wavelength and all-messenger DWF programme dataset searching for extragalactic fast transients. Hundreds to thousands of astronomical transient and variable sources were discovered in DECam optical data, 9 of which (see Table 4) passed strict selection criteria, described in Section 3.1. Those eFTCs (extragalactic fast transient candidates) are well constrained in time, within observing windows of ∼1 hr, and appear not to be coincident with stellar sources. Adding optical multi-band star/galaxy separation measurements to g-band information, we were able to confidently label 5 of those as stellar flares with faint quiescent counterparts. Four eFTCs (DWF17k, DWF17x, DWF17ao, DWF17ax) may be Galactic flares but their classification remains uncertain. With simultaneous (and near-simultaneous) multi-wavelength observations we did not identify fast radio bursts using the Parkes and Molonglo radio telescopes, or gamma-ray events associated with those eFTCs using the *Swift* and *Fermi* satellites. Those eFTC showed no significant long-term variability detectable at approximate $i = 20.27, z = 19.42, u = 19.34, v = 19.59, g = 21.57, r = 21.25$ magnitude limits.

We have estimated areal rates of extragalactic fast transients at timescales ranging between 1.17 and 52.0 minutes, between $23 \lesssim g \lesssim 24.7$ survey limiting magnitudes. Firstly, we assumed that all our detections are Galactic flares, which is the most likely scenario, and we place rate upper limits (Table A1) in new regimes of the 'deep and fast' region of the phase space. Secondly, we calculate rates (Table 7) assuming that 4 sources DWF17k, DWF17x, DWF17ao, DWF17ax occurred outside the Milky Way.

In large surveys focused on extragalactic astronomy, fast optical transients may be rejected as 'contaminant' stellar flares based on their light curve. However, we showed that light curves of confirmed extragalactic fast transients (such as the prompt optical flash of GRB110205A) can mimic the behaviour of Galactic flare star light curves. This fact suggests that more solid criteria than 'hostless' and 'with flare-star-like light curve' should always be adopted when searching for extragalactic transients in optical surveys. Simultaneous multi-wavelength and multi-messenger observations, along with rapid detection and prompt or long-term follow up is key to characterising the fast transient sky. Future DWF programme observations can further improve our understanding of the minute-timescale transient sky in the optical, as well as unveil the nature of the fastest bursts across several bands of the electromagnetic spectrum and using multiple messengers.

ACKNOWLEDGEMENTS

We thank the *Swift* team that helped maximize the observability of DWF target fields with BAT with optimized scheduling of the satellite. We thank Vivek Venkatraman Krishnan for helping with Molonglo operations. We thank the SUPERB (SUrvey for Pulsars and Extragalactic Radio Bursts) team who coordinated Parkes with other DWF facilities for simultaneous observations. We thank Breakthrough Listen, who collaborated with flexible rescheduling of Parkes observing time to benefit DWF multi-facility coordination.
Part of this research was funded by the Australian Research Council Centre of Excellence for Gravitational Wave Discovery (OzGrav), CE170100004 and the Australian Research Council Centre of Excellence for All-sky Astrophysics (CAASTRO), CE110001020.
Research support to IA is provided by the Australian Astronomical Observatory (AAO). Research support to IA is also provided by the GROWTH project, funded by the National Science Foundation under Grant No 1545949. GROWTH is a collaborative project between California Institute of Technology (USA), Pomona College (USA), San Diego State University (USA), Los Alamos National Laboratory (USA), University of Maryland College Park (USA), University of Wisconsin Milwaukee (USA), Tokyo Institute of Technology (Japan), National Central University (Taiwan), Indian Institute of Astrophysics (India), Inter-University Center for Astronomy and Astrophysics (India), Weizmann Institute of Science (Israel), The Oskar Klein Centre at Stockholm University (Sweden), Humboldt University (Germany).
JC acknowledges the Australian Research Council Future Fellowship grant FT130101219.
This work has made use of data from the European Space Agency (ESA) mission *Gaia* (`https://www.cosmos.esa.int/gaia`), processed by the *Gaia* Data Processing and Analysis Consortium (DPAC, `https://www.cosmos.esa.int/web/gaia/dpac/consortium`). Funding for the DPAC has been provided by national institutions, in particular the

institutions participating in the *Gaia* Multilateral Agreement.

The national facility capability for SkyMapper has been funded through ARC LIEF grant LE130100104 from the Australian Research Council, awarded to the University of Sydney, the Australian National University, Swinburne University of Technology, the University of Queensland, the University of Western Australia, the University of Melbourne, Curtin University of Technology, Monash University and the Australian Astronomical Observatory. SkyMapper is owned and operated by The Australian National University's Research School of Astronomy and Astrophysics.

This project used data obtained with the Dark Energy Camera (DECam), which was constructed by the Dark Energy Survey (DES) collaboration. Funding for the DES Projects has been provided by the U.S. Department of Energy, the U.S. National Science Foundation, the Ministry of Science and Education of Spain, the Science and Technology Facilities Council of the United Kingdom, the Higher Education Funding Council for England, the National Center for Supercomputing Applications at the University of Illinois at Urbana-Champaign, the Kavli Institute of Cosmological Physics at the University of Chicago, the Center for Cosmology and Astro-Particle Physics at the Ohio State University, the Mitchell Institute for Fundamental Physics and Astronomy at Texas A&M University, Financiadora de Estudos e Projetos, Fundação Carlos Chagas Filho de Amparo à Pesquisa do Estado do Rio de Janeiro, Conselho Nacional de Desenvolvimento Científico e Tecnológico and the Ministério da Ciência, Tecnologia e Inovacão, the Deutsche Forschungsgemeinschaft, and the Collaborating Institutions in the Dark Energy Survey. The Collaborating Institutions are Argonne National Laboratory, the University of California at Santa Cruz, the University of Cambridge, Centro de Investigaciones Enérgeticas, Medioambientales y Tecnológicas-Madrid, the University of Chicago, University College London, the DES-Brazil Consortium, the University of Edinburgh, the Eidgenössische Technische Hochschule (ETH) Zürich, Fermi National Accelerator Laboratory, the University of Illinois at Urbana-Champaign, the Institut de Ciències de l'Espai (IEEC/CSIC), the Institut de Física d'Altes Energies, Lawrence Berkeley National Laboratory, the Ludwig-Maximilians Universität München and the associated Excellence Cluster Universe, the University of Michigan, the National Optical Astronomy Observatory, the University of Nottingham, the Ohio State University, the OzDES Membership Consortium the University of Pennsylvania, the University of Portsmouth, SLAC National Accelerator Laboratory, Stanford University, the University of Sussex, and Texas A&M University. Based on observations at Cerro Tololo Inter-American Observatory, National Optical Astronomy Observatory which is operated by the Association of Universities for Research in Astronomy (AURA) under a cooperative agreement with the National Science Foundation.

REFERENCES

Abbott B., et al., 2017, ApJL, 848, L12
Andreoni I., Cooke J., 2018, ArXiv e-print 1802.01100v1
Andreoni I., Jacobs C., Hegarty S., Pritchard T., Cooke J., Ryder S., 2017, PASA, 34, e037
Arcavi I., 2018, ApJ, 855, L23
Arcavi I., et al., 2016, ApJ, 819, 35
Arcavi I., et al., 2017, Nature, 551, 64
Astier P., et al., 2006, A&A, 447, 31
Bailes M., et al., 2017, Publications of the Astronomical Society of Australia, 34, e045
Barthelmy S. D., et al., 2005, SSRv, 120, 143
Becker A. C., et al., 2004, ApJ, 611, 418
Bellm E. C., et al., 2019, Publications of the Astronomical Society of the Pacific, 131, 018002
Berger E., Fong W., Chornock R., 2013a, ApJL, 774, L23
Berger E., et al., 2013b, ApJ, 779, 18
Bersten M. C., et al., 2018, preprint, (arXiv:1802.09360)
Bertin E., Arnouts S., 2010, SExtractor: Source Extractor, Astrophysics Source Code Library (ascl:1010.064)
Cenko S. B., 2017, Nature Astronomy, 1, 0008
Cenko S. B., et al., 2015, ApJL, 803, L24
Coulter D. A., et al., 2017, Science, 358, 1556
Cowperthwaite P. S., et al., 2017, ApJ, 848, L17
Cowperthwaite P. S., et al., 2018, ApJ, 858, 18
Cucchiara A., et al., 2011, ApJ, 743, 154
Dark Energy Survey Collaboration et al., 2016, MNRAS, 460, 1270
Davenport J. R. A., et al., 2014, ApJ, 797, 122
De K., et al., 2018, Science, 362, 201
Doctor Z., et al., 2017, ApJ, 837, 57
Drake A. J., et al., 2009, ApJ, 696, 870
Drout M. R., et al., 2014, ApJ, 794, 23
Farah W., et al., 2018, MNRAS, 478, 1209
Flaugher B., et al., 2015, AJ, 150, 150
Förster F., et al., 2016, ApJ, 832, 155
Fox D. W., et al., 2003, ApJ, 586, L5
Gaia Collaboration et al., 2016, A&A, 595, A1
Gaia Collaboration Brown A. G. A., Vallenari A., Prusti T., de Bruijne J. H. J., Babusiaux C., Bailer-Jones C. A. L., 2018, preprint, (arXiv:1804.09365)
Gao H., Ding X., Wu X.-F., Dai Z.-G., Zhang B., 2015, ApJ, 807, 163
Garnavich P. M., Tucker B. E., Rest A., Shaya E. J., Olling R. P., Kasen D., Villar A., 2016, ApJ, 820, 23
Gehrels N., 1986, ApJ, 303, 336
Hamuy M., Pinto P. A., 1999, AJ, 117, 1185
Hardy L. K., et al., 2017, MNRAS, 472, 2800
Henden A. A., Templeton M., Terrell D., Smith T. C., Levine S., Welch D., 2016, VizieR Online Data Catalog, 2336
Ho A. Y. Q., et al., 2018, ApJ, 854, L13
Holoien T. W.-S., et al., 2017, MNRAS, 471, 4966
Jin Z.-P., Li X., Cano Z., Covino S., Fan Y.-Z., Wei D.-M., 2015, ApJ, 811, L22
Jin Z.-P., et al., 2016, Nature Communications, 7, 12898
Jin Z.-P., Covino S., Liao N.-H., Li X., D'Avanzo P., Fan Y.-Z., Wei D.-M., 2019, arXiv e-prints, p. arXiv:1901.06269
Kasliwal M. M., et al., 2010, ApJ, 723, L98
Kasliwal M. M., et al., 2017, Science, 358, 1559
Keane E. F., Petroff E., 2015, MNRAS, 447, 2852
Keane E. F., et al., 2018, MNRAS, 473, 116
Keith M. J., et al., 2010, MNRAS, 409, 619
Keller S. C., et al., 2007, PASA, 24, 1
Kowalski A. F., Hawley S. L., Hilton E. J., Becker A. C., West A. A., Bochanski J. J., Sesar B., 2009, AJ, 138, 633
LSST Science Collaboration et al., 2009, arXiv e-prints, p. arXiv:0912.0201
Lipunov V. M., et al., 2007, Astronomy Reports, 51, 1004
Lipunov V., et al., 2017, ApJ, 850, L1
Lorimer D. R., Bailes M., McLaughlin M. A., Narkevic D. J., Crawford F., 2007, Science, 318, 777

Martin-Carrillo A., et al., 2014, A&A, 567, A84
Meegan C., et al., 2009, ApJ, 702, 791
Perley D. A., et al., 2009, ApJ, 696, 1871
Poznanski D., et al., 2010, Science, 327, 58
Price D. C., Staveley-Smith L., Bailes M., Carretti E., Jameson A., Jones M. E., van Straten W., Schediwy S. W., 2016, Journal of Astronomical Instrumentation, 5, 1641007
Pursiainen M., et al., 2018, preprint, (arXiv:1803.04869)
Rau A., Ofek E. O., Kulkarni S. R., Madore B. F., Pevunova O., Ajello M., 2008, ApJ, 682, 1205
Rau A., et al., 2009, PASP, 121, 1334
Rest A., et al., 2018, Nature Astronomy, 2, 307
Rodney S. A., et al., 2018, Nature Astronomy, 2, 324
Rubin A., Gal-Yam A., 2017, ApJ, 848, 8
Rykoff E. S., et al., 2005, ApJ, 631, 1032
Scalzo R. A., et al., 2017, PASA, 34, e030
Shappee B. J., et al., 2014, ApJ, 788, 48
Shivvers I., et al., 2016, MNRAS, 461, 3057
Soares-Santos M., et al., 2017, ApJ, 848, L16
Sokołowski M., Małek K., Piotrowski L. W., Wrochna G., 2010, Advances in Astronomy, 2010, 463496
Staveley-Smith L., et al., 1996, PASA, 13, 243
Stubbs C. W., Doherty P., Cramer C., Narayan G., Brown Y. J., Lykke K. R., Woodward J. T., Tonry J. L., 2010, ApJS, 191, 376
Swaters R. A., Valdes F. G., 2007, in Shaw R. A., Hill F., Bell D. J., eds, Astronomical Society of the Pacific Conference Series Vol. 376, Astronomical Data Analysis Software and Systems XVI. p. 269
Tanaka M., et al., 2016, ApJ, 819, 5
Tanvir N. R., Levan A. J., Fruchter A. S., Hjorth J., Hounsell R. A., Wiersema K., Tunnicliffe R. L., 2013, Nature, 500, 547
Tanvir N. R., et al., 2017, ApJ, 848, L27
Tendulkar S. P., et al., 2017, ApJ, 834, L7
Troja E., et al., 2017, Nature, 547, 425
Troja E., et al., 2018, Nature Communications, 9, 4089
Valdes F. G., Swaters R. A., 2007, in Shaw R. A., Hill F., Bell D. J., eds, Astronomical Society of the Pacific Conference Series Vol. 376, Astronomical Data Analysis Software and Systems XVI. p. 273
Valenti S., et al., 2017, ApJ, 848, L24
Vestrand W. T., et al., 2014, Science, 343, 38
Villar V. A., et al., 2017, ApJ, 851, L21
West A. A., et al., 2011, AJ, 141, 97
Wolf C., et al., 2018, PASA, 35, e010
van Roestel J., et al., 2019, MNRAS, 484, 4507

APPENDIX A: UPPER LIMITS FOR AREAL RATES

In this table we report upper limits for the rate of optical extragalactic fast transients. The rates are obtained as explained in Section 6 and are plotted in Figure 6.

Timescale (minutes)	Rate upper limits (events day^{-1} deg^{-2})				
	23.0	**23.7**	**24.2**	**24.5**	**24.7**
1.17	1.625				
2.0	1.422				
2.83	1.294				
3.67	1.250				
4.5	1.222				
5.33	1.203				
6.17	1.189				
7.0	1.179				
7.83	1.170	5.77			
8.67	1.164				
9.5	1.158				
10.33	1.153				
11.17	1.149				
12.0	1.146	5.65			
12.83	1.143				
13.67	1.140				
14.5	1.138		9.81		
15.33	1.136				
16.17	1.134	5.60			
17.0	1.132				
17.83	1.131				
18.67	1.130				
19.5	1.128				
20.33	1.127	5.56			
21.17	1.126			13.59	
22.0	1.125		9.70		
22.83	1.124				
23.67	1.123				
24.5	1.123	5.54			
25.33	1.122				
26.17	1.121				
27.0	1.120				
27.83	1.120				17.03
28.67	1.119	5.52			
29.5	1.119		9.64		
30.33	1.118				
31.17	1.118				
32.0	1.117			13.48	
32.83	1.117	5.51			
33.67	1.116				
34.5	1.116				
35.33	1.116				
36.17	1.115				
37.0	1.115	5.50	9.61		
37.83	1.115				
38.67	1.114				
39.5	1.114				
40.33	1.114				
41.17	1.113	5.49			
42.0	1.113				16.92
42.83	1.113			13.43	
43.67	1.113				
44.5	1.112		9.59		
45.33	1.112	5.49			
46.17	1.112				
47.0	1.112				
47.83	1.112				
48.67	1.111				
49.5	1.111	5.48			
50.33	1.111				

51.17	1.111	
52.0	1.111	
52.83	1.110	
53.67	1.110	5.48
54.5	1.110	
55.33	1.110	
56.17	1.110	
57.0	1.110	
57.83	1.110	
58.67	1.109	
59.5	1.109	

APPENDIX B: SKYMAPPER PHOTOMETRY

Photometry obtained by the SkyMapper telescope (Keller et al. 2007) around the dates of the Deeper, Wider, Faster programmes. Photometric measurements are obtained from raw or subtracted images (see origin column) depending on template and coverage availabilityusing the SkyMapper Transient Survey pipeline (Scalzo et al. 2017).

candidate	date (UTC)	filter	mag	mag_err	maglim_arr	origin
DWF17a	2017-02-07T16:31:59	*g*	-	-	19.56	raw
DWF17a	2017-02-07T16:53:51	*r*	-	-	20.43	raw
DWF17a	2017-02-22T12:01:39	*g*	-	-	21.48	raw
DWF17a	2017-02-22T12:25:17	*r*	-	-	21.11	raw
DWF17a	2017-02-27T11:52:05	*g*	-	-	21.46	raw
DWF17a	2017-02-27T13:17:48	*r*	-	-	21.20	raw
DWF17a	2017-03-08T15:53:42	*g*	-	-	20.27	raw
DWF17a	2018-06-11T09:15:26	*g*	-	-	21.06	raw
DWF17a	2018-06-11T09:17:29	*g*	-	-	21.05	raw
DWF17a	2018-06-11T09:19:30	*r*	-	-	20.63	raw
DWF17a	2018-06-11T09:21:30	*r*	-	-	20.57	raw
DWF17a	2018-06-21T08:49:19	*r*	-	-	20.28	raw
DWF17a	2018-06-21T08:51:19	*g*	-	-	20.24	raw
DWF17a	2018-06-25T08:43:13	*g*	-	-	20.17	raw
DWF17a	2018-06-25T08:45:13	*r*	-	-	20.29	raw
DWF17c	2017-02-07T16:31:59	*g*	-	-	19.28	raw
DWF17c	2017-02-07T16:53:51	*r*	-	-	20.11	raw
DWF17c	2017-02-22T12:01:39	*g*	-	-	21.42	raw
DWF17c	2017-02-22T12:25:17	*r*	-	-	20.88	raw
DWF17c	2017-02-27T11:52:05	*g*	-	-	21.42	raw
DWF17c	2017-02-27T13:17:48	*r*	-	-	21.06	raw
DWF17c	2017-03-08T15:53:42	*g*	-	-	20.17	raw
DWF17c	2018-06-11T09:15:26	*g*	-	-	21.00	raw
DWF17c	2018-06-11T09:17:29	*g*	-	-	21.00	raw
DWF17c	2018-06-11T09:19:30	*r*	-	-	20.59	raw
DWF17c	2018-06-11T09:21:30	*r*	-	-	20.48	raw
DWF17c	2018-06-21T08:49:19	*r*	-	-	20.20	raw
DWF17c	2018-06-21T08:51:19	*g*	-	-	20.13	raw
DWF17c	2018-06-25T08:43:13	*g*	-	-	20.13	raw
DWF17c	2018-06-25T08:45:13	*r*	-	-	20.21	raw
DWF17f	2017-02-07T16:31:59	*g*	-	-	19.46	raw
DWF17f	2017-02-07T16:53:51	*r*	-	-	20.19	raw
DWF17f	2017-02-22T12:01:39	*g*	-	-	21.36	raw
DWF17f	2017-02-22T12:25:17	*r*	-	-	20.92	raw
DWF17f	2017-02-27T11:52:05	*g*	-	-	21.36	raw
DWF17f	2017-02-27T13:17:48	*r*	-	-	21.05	raw
DWF17f	2017-03-08T15:53:42	*g*	-	-	20.22	raw
DWF17f	2018-06-11T09:15:26	*g*	-	-	20.99	raw
DWF17f	2018-06-11T09:17:29	*g*	-	-	21.10	raw
DWF17f	2018-06-11T09:19:30	*r*	-	-	20.64	raw
DWF17f	2018-06-11T09:21:30	*r*	-	-	20.46	raw
DWF17f	2018-06-21T08:49:19	*r*	-	-	20.28	raw
DWF17f	2018-06-21T08:51:19	*g*	-	-	20.23	raw
DWF17f	2018-06-25T08:43:13	*g*	-	-	20.15	raw
DWF17f	2018-06-25T08:45:13	*r*	-	-	20.21	raw
DWF17g	2017-02-07T16:31:59	*g*	-	-	19.56	raw

DWF17g	2017-02-07T16:53:51	*r*	-	-	20.43	raw
DWF17g	2017-02-22T12:01:39	*g*	21.02	0.10	21.48	raw
DWF17g	2017-02-22T12:25:17	*r*	20.18	0.07	21.11	raw
DWF17g	2017-02-27T11:52:05	*g*	21.24	0.12	21.46	raw
DWF17g	2017-02-27T13:17:48	*r*	20.21	0.06	21.20	raw
DWF17g	2017-03-08T15:53:42	*g*	-	-	20.27	raw
DWF17g	2018-06-11T09:15:26	*g*	-	-	21.06	raw
DWF17g	2018-06-11T09:17:29	*g*	-	-	21.05	raw
DWF17g	2018-06-11T09:19:30	*r*	-	-	20.63	raw
DWF17g	2018-06-11T09:21:30	*r*	-	-	20.57	raw
DWF17g	2018-06-21T08:49:19	*r*	-	-	20.28	raw
DWF17g	2018-06-21T08:51:19	*g*	-	-	20.24	raw
DWF17g	2018-06-25T08:43:13	*g*	-	-	20.17	raw
DWF17g	2018-06-25T08:45:13	*r*	-	-	20.29	raw
DWF17k	2017-01-21T11:07:04	*g*	-	-	20.98	raw
DWF17k	2017-01-21T11:09:04	*r*	-	-	20.73	raw
DWF17k	2017-01-22T10:55:04	*g*	-	-	21.37	raw
DWF17k	2017-01-22T10:57:04	*r*	-	-	20.87	raw
DWF17k	2017-02-12T10:33:07	*v*	-	-	16.86	raw
DWF17k	2017-02-13T10:41:16	*v*	-	-	18.51	raw
DWF17k	2017-02-13T10:43:17	*v*	-	-	19.11	raw
DWF17k	2017-02-13T10:45:18	*v*	-	-	18.98	raw
DWF17k	2017-02-13T10:47:18	*v*	-	-	18.04	raw
DWF17k	2017-02-14T13:02:15	*v*	-	-	18.48	raw
DWF17k	2017-02-14T13:04:15	*v*	-	-	18.44	raw
DWF17k	2017-02-14T13:08:16	*v*	-	-	18.28	raw
DWF17k	2017-02-20T10:49:12	*v*	-	-	19.55	raw
DWF17k	2017-02-20T10:51:12	*v*	-	-	18.77	raw
DWF17k	2017-02-27T10:15:52	*g*	-	-	21.46	raw
DWF17k	2017-02-27T10:40:47	*r*	-	-	21.10	raw
DWF17k	2017-02-27T10:15:52	*g*	-	-	21.46	sub
DWF17k	2017-02-27T10:40:47	*r*	-	-	21.10	sub
DWF17x	2017-01-21T11:07:04	*g*	-	-	20.81	raw
DWF17x	2017-01-21T11:09:04	*r*	-	-	20.71	raw
DWF17x	2017-01-22T10:55:04	*g*	-	-	21.27	raw
DWF17x	2017-01-22T10:57:04	*r*	-	-	20.72	raw
DWF17x	2017-02-12T10:33:07	*v*	-	-	16.87	raw
DWF17x	2017-02-13T10:41:16	*v*	-	-	18.48	raw
DWF17x	2017-02-13T10:43:17	*v*	-	-	19.07	raw
DWF17x	2017-02-13T10:45:18	*v*	-	-	18.99	raw
DWF17x	2017-02-13T10:47:18	*v*	-	-	17.83	raw
DWF17x	2017-02-14T13:02:15	*v*	-	-	18.42	raw
DWF17x	2017-02-14T13:04:15	*v*	-	-	18.41	raw
DWF17x	2017-02-14T13:08:16	*v*	-	-	18.17	raw
DWF17x	2017-02-20T10:49:12	*v*	-	-	19.40	raw
DWF17x	2017-02-20T10:51:12	*v*	-	-	18.48	raw
DWF17x	2017-02-27T10:15:52	*g*	-	-	21.35	raw
DWF17x	2017-02-27T10:40:47	*r*	-	-	21.00	raw
DWF17x	2017-02-27T10:15:52	*g*	-	-	21.35	sub
DWF17x	2017-02-27T10:40:47	*r*	-	-	21.00	sub
DWF17ao	2017-01-22T10:51:03	*g*	-	-	21.57	raw
DWF17ao	2017-01-22T10:53:03	*r*	-	-	21.25	raw
DWF17ao	2017-02-27T10:13:52	*g*	-	-	21.52	raw
DWF17ao	2017-02-27T10:38:47	*r*	-	-	21.09	raw
DWF17ao	2017-02-27T10:13:52	*g*	-	-	21.52	sub
DWF17ao	2017-02-27T10:38:47	*r*	-	-	21.09	sub
DWF17ax	2017-01-21T11:03:02	*g*	-	-	21.43	raw
DWF17ax	2017-01-21T11:05:03	*r*	-	-	20.93	raw
DWF17ax	2017-01-22T10:51:03	*g*	-	-	21.46	raw
DWF17ax	2017-01-22T10:53:03	*r*	-	-	21.23	raw
DWF17ax	2017-02-27T10:13:52	*g*	-	-	21.42	raw
DWF17ax	2017-02-27T10:38:47	*r*	-	-	21.03	raw
DWF17ax	2017-02-27T10:13:52	*g*	-	-	21.42	sub
DWF17ax	2017-02-27T10:38:47	*r*	-	-	21.03	sub